UNIVERSITY OF HELSINKI REPORT SERIES IN PHYSICS

HU-P-D212

Low-energy radiation effects in polyethylene and cellulose

Jussi Polvi

Division of Materials Physics
Department of Physics
Faculty of Science
University of Helsinki
Helsinki, Finland

ACADEMIC DISSERTATION

To be presented with the permission of the Faculty of Science of the University of Helsinki, for public criticism in Lecture hall 5 of the Main Building of the University of Helsinki, on December 21st 2013, at 12 o'clock noon.

HELSINKI 2013

ISBN 978-952-10-8946-6 (printed version)
ISSN 0356-0961
Helsinki 2013
Unigrafia Oy

ISBN 978-952-10-8947-3 (PDF version)
http://ethesis.helsinki.fi
Helsinki 2013
Electronic Publications @ University of Helsinki (Helsingin yliopiston verkkojulkaisut)

Jussi Polvi, **Low-energy radiation effects in polyethylene and cellulose**, University of Helsinki, 2013, 56 p. + appendices, University of Helsinki Report Series in Physics, HU-P-D212, ISSN 0356-0961, ISBN 978-952-10-8946-6 (printed version), ISBN 978-952-10-8947-3 (PDF version)

ABSTRACT

Polymers are found everywhere in daily life. Natural polymers, such as wood, wool, cotton and silk have been used by humans for centuries. During the past hundred years, synthetic polymers have taken over from previous structural materials such as wood, stone, iron or glass, and today most of the tools and containers used at home are made of, at least partly, different plastics.

This thesis concentrates on studying irradiation effects in two polymers, polyethylene and cellulose. Polyethylene (PE) is the most commonly used synthetic polymer and plastic bottles, pipes, films, toys and food packages are usually made of different brands of PE. As for cellulose, it is the most abundant natural polymer on Earth and almost all plant life contains large amounts of cellulose.

Irradiation has been widely used by the industry to process and modify synthetic polymers such as PE since the 1950s. The earliest applications were cross-linking of plastic materials, sterilizing medical equipment and preserving food products, and since then, many more practical applications for radiation processed materials have been developed. Recently there has been a rise of interest in the usage of irradiation in relation to wood products. Since the most abundant molecule in wood is cellulose, this raises an interest in understanding radiation effects in cellulose.

Even though irradiation is nowadays widely used in processing of both synthetic and natural polymers, the atomic level description of the physics of irradiation effects in these materials is still very much incomplete. The focus of this thesis is to examine the mechanism of irradiation induced defect formation in high-density polyethylene and cellulose on 10^{-10} m length scale using molecular dynamics simulations. The results presented in this thesis provide a unique atomic-level view into the reactions initiated by irradiation in polymers, such as chain scission, radical formation and cross-linking.

ACKNOWLEDGEMENTS

I wish to thank the head of the Department of Physics, Prof. Juhani Keinonen, and the head of the Accelerator Laboratory, Prof. Jyrki Räisänen, for providing the facilities for the research presented in this thesis. Financial support from the Academy of Finland and Waldemar von Frenckells stiftelse are gratefully acknowledged.

I thank Prof. Ilpo Vattulainen and Dr. Emppu Salonen for the pre-examination of my thesis and their many insightful comments. I am also thankful to Prof. Erik Neyts for agreeing to be my opponent in the public examination of this thesis.

I am deeply grateful to my supervisor, Prof. Kai Nordlund, for being a never-ending source of good ideas and inspiration. Usually after a good discussion with Kai, your next article is suddenly half-finished and the thesis is only just a couple of weeks away.

During my first stages at the lab, I had the fortune of having Tommi Järvi as my co-supervisor. Tommi provided me a great role model for a good scientist: always be 'noheva', meaning; talk straight, answer your emails, and always check that the science in your simulations makes sense.

I also want to thank Antti Kuronen for all the good discussions over lunch or beer, and for demonstrating that it is apparently possible to find a position at the university where most of your work is not paperwork and bureaucracy, but teaching and physics.

Many of my colleagues at the lab are not just that, but true friends also. I thank you all for these past years. Special thanks to Lotta, for being my best critic, a general source of wisdom, and for constantly pushing me to be a better man; to Ane, for being so... you; and to Laura, for allowing me to work at the lab sharing a room with a friend.

I am thankful to all my friends outside the lab for keeping most of my weekends busy. You give my life a balance, you keep me sane.

To my parents and grandparents, I owe you for everything that I am.

Helsinki, October 26th, 2013

Jussi

Contents

ABSTRACT **iii**

ACKNOWLEDGEMENTS **iv**

1 INTRODUCTION **1**

2 PURPOSE AND STRUCTURE **3**

2.1 Summaries of the original publications 3

2.2 Author's contribution 5

3 POLYMERS **6**

3.1 Overview 6

3.2 Polyethylene 8

3.2.1 Types of polyethylene 8

3.3 Cellulose 10

3.3.1 General properties 11

3.3.2 Different crystal structures 11

4 LOW-ENERGY RADIATION EFFECTS IN SOLIDS **13**

4.1 Overview 13

4.2 Electronic and nuclear stopping 15

4.3 Radiation effects in polymers 16

4.3.1 Polyethylene and irradiation 17

4.3.2 Cellulose and irradiation 18

5 COMPUTATIONAL METHODS **20**

5.1 Molecular dynamics 20

5.1.1 Simulation algorithms 20

5.1.2 Inter-atomic potentials 22

5.2 Simulation set-up 25

6 RESULTS **29**

6.1 Threshold energy for damage production 29

6.1.1 Polyethylene 29

6.1.2 Cellulose 31

6.1.3 Discussion 32

6.2 Damage production above the threshold energy 34

6.2.1 Polyethylene 35

6.2.2 Cellulose 37

6.2.3 Discussion 39

7 CONCLUSIONS **41**

REFERENCES **42**

1 INTRODUCTION

Polyethylene and cellulose are found in abundance everywhere around you. Polyethylene (PE) is the most commonly used synthetic polymer, its annual production being approximately 80 million tons [70]. Plastic bottles, toys and food packages are usually made of high-density polyethylene (HDPE), and, in general, whenever you are talking about plastics there is about a 50% chance that you are actually referring to polyethylene. As for cellulose, it is the main component of plant cell walls and almost all plant life contains large amounts of cellulose; for instance, wood typically consists of 40-45% cellulose [84].

Polymeric materials such as plastics and rubber are subject to irradiation in nature due to ultraviolet light from the sun, and its long term effects can be seen in old and brittle plastic toys (see Fig. 1) or cracking old tires. Irradiation has also been deliberately used to process and modify polymeric materials by the industry for almost half a century [36]. The earliest applications were cross-linking plastic materials, sterilizing medical equipment and preserving food products. Since then, many more practical applications for radiation processed materials have been developed. For instance, electron beam cross-linking of synthetic polymers like PE can be used to produce heat-shrinkable plastic films for packaging foods, or plastic foams and hydrogels for medical applications [76, 26].

Figure 1: A plastic toy made brittle by long exposure to radiation.

Recently there has been a rise of interest in the usage of irradiation in relation to wood products. For instance, plasmas can be used to modify the water absorbance of wood surfaces [91, 12, 97, 8, 9], and recent work has shown that also electron beam irradiation at 150 keV can have similar effects [94]. Since the most abundant molecule in wood is cellulose, this raises an interest in understanding radiation effects in cellulose.

Even though irradiation is nowadays widely used in the processing of both synthetic and natural polymers, the atomic level description of the physics of irradiation effects in these materials is still very much incomplete. There are many reasons for this: organic materials are difficult to characterize because of their often complex atomic structure, especially in comparison to metals, and the complex structure leads to complex effects such as chain scission, radical formation and cross-linking. Due to these reasons, the computational modelling of irradiation effects in organic materials is more complicated

than the modelling of irradiation effects in metals, and good tools for that purpose, such as AIREBO [86, 17] and ReaxFF [90], have only become available quite recently.

The focus of this thesis is to examine the atomic level mechanism of irradiation induced defect formation in HDPE and cellulose by using atomistic molecular dynamics (MD) simulations. A considerable number of experimental studies relating to radiation chemistry and physics of PE [23, 22, 82, 45, 46, 69] have been published but only a few computational studies are available [11, 30, 99]. The irradiation of cellulose has been a subject of study in some recent articles [49, 88, 93, 28] but MD simulations have not been previously used. The first part of the results, presented in Section 6.1 of this thesis, is focused on the threshold energy for damage production in both polyethylene and cellulose. This part will shed some light on questions related to the radiation resistance of these materials. The second part of the results, Section 6.2, will concentrate on the damage production above the threshold energy, studying the effects of both single recoil events and damage build-up from consecutive recoil impacts on HDPE or cellulose samples.

2 PURPOSE AND STRUCTURE

The goal of this thesis is to provide a better understanding of the atomistic mechanism of defect formation as a result of low-energy radiation in organic materials. For this purpose molecular dynamics simulations have been used to study the details of the irradiation process in high-density polyethylene and cellulose Iβ. The results presented in this thesis provide a unique atomic-level view into the reactions initiated by irradiation in polymers, such as chain scission, radical formation and cross-linking.

This thesis consists of this summary and five publications. The five publications are referred to by bold-face Roman numerals. The structure of the thesis is as follows. In this section, the five publications are summarized and the author's contributions are explained. In section 3, a general overview of polymers and more detailed descriptions of polyethylene and cellulose are presented. Low energy irradiation effects in solids are discussed in section 4. Section 5 describes the computational methods used in this thesis. In section 6 the main results of this thesis are provided. First the results from the damage threshold simulations are outlined and then the results from simulations of damage production above the threshold energy. Finally, conclusions are presented in section 7.

2.1 Summaries of the original publications

Publication I: Primary Radiation Defect Production in Polyethylene and Cellulose

J. Polvi, P. Luukkonen, T. T. Järvi, T. W. Kemper, S. B. Sinnott, and K. Nordlund, *Journal of Physical Chemistry B* **116**, 13932-13938 (2012) [71]

Irradiation effects in polyethylene and cellulose were examined using molecular dynamics simulations. The governing reactions in both materials were chain scissioning and generation of small hydrocarbon and peroxy radicals. Recombination of chain fragments and cross-linking between polymer chains were found to occur less frequently. Crystalline cellulose was found to be more resistant to radiation damage than crystalline polyethylene. Statistics on radical formation are presented and the dynamics of the formation of radiation damage discussed.

Publication II: Irradiation effects in high-density polyethylene

J. Polvi and K. Nordlund, *Nuclear Instruments and Methdods in Physics Research B* **312**, 54-59 (2013) [73]

Using molecular dynamics simulations, we have studied the irradiation effects in high density polyethylene. We found that the governing reactions were chain scissioning and generation of free radicals, whereas cross-linking and recombination of chain fragments

was rare. We also determined the threshold energy for creating defects in the polyethylene lattice as a function of the recoil angle. Our analysis on the damage threshold energy shows that it is strongly dependent on the initial recoil direction and on average two times higher for the carbon atoms than for the hydrogen atoms in the polyethylene chain.

Publication III: Self-recoil irradiation effects in crystalline polyethylene
J. Polvi and K. Nordlund, *Proceedings of the 2013 Ion-Solid Interactions conference*, Volume 2, 69-73, Moscow aviation institute publisher, Moscow, Russia (2013) [75]

In order to get insight into the atomistic mechanism of cross-linking, we examine here irradiation-induced defects in crystalline high density polyethylene, using molecular dynamics simulations. Polyethylene is the structurally and conceptually the simplest of organic polymers, and experimentally HDPE has been observed to have high tendency for cross-linking. Our results illustrate the probability and nature of damage produced by low-energy recoils in HDPE.

Publication IV: Comparison of low-energy β radiation effects in polyethylene and cellulose by molecular dynamics simulations
J. Polvi and K. Nordlund, *NIMB Proceedings: The 17th International Conference on Radiation Effects in Insulators*, (2013), Accepted for publication [72]

Using molecular dynamics simulations, we have compared the low-energy β radiation effects in high density polyethylene and cellulose. We determined the threshold energy for creating defects as a function of the recoil direction, for a carbon atom in the polyethylene chain, and for one of the carbon atoms in the cellulose chain. Our analysis shows that the damage threshold energy is in both cases strongly dependent on the initial recoil direction and on average slightly higher for the carbon atoms in the polyethylene chain than for the target carbon atom in the cellulose chain. Additionally we performed two sets of recoil event simulations in polyethylene sample, with 50 and 100 eV recoil energy, and compared the outcome with previously reported recoil event results from cellulose simulations.

Publication V: Low-energy irradiation effects in cellulose
J. Polvi and K. Nordlund, *Journal of Applied Physics*, (2013), Submitted for publication [74]

Using molecular dynamics simulations, we determined the threshold energy for creating defects as a function of the incident angle, for all carbon and oxygen atoms in the cellulose monomer. Our analysis shows that the damage threshold energy is strongly dependent on the initial recoil direction and on average slightly higher for oxygen atoms than for carbon atoms in cellulose. We also performed cumulative bombardment simulations mimicking low-energy electron irradiation (such as TEM imaging) on cellulose and analysed the resulting damage.

2.2 Author's contribution

The author carried out all the simulations in publications **II-V** while in publication **I**, a part of the polyethylene simulations were done by Petri Luukkonen. Analysis of the results and writing of the manuscripts was mainly carried out by the author for all publications.

Other work

In addition to publications included in this thesis, the author has contributed to the following article:

In connection to the publication [43], the author performed molecular dynamics simulations on ethylene carbonate and propylene carbonate liquids to get properly relaxed input systems for the tight-binding simulations performed there. The author also wrote the part describing these MD simulations in the article.

3 POLYMERS

3.1 Overview

A *polymer* is a large molecule composed of many repeated subunits, known as monomers. The term polymer derives from the Greek 'poly' meaning 'many' and 'mer' meaning units. Polymers are formed by linking a large number of small molecules together. Perhaps the simplest example of a polymer is polyethylene $(CH_2\text{-}CH_2)_n$, shown in Fig. 2, which can be viewed as an extension of usual, fully saturated hyrdocarbons of form C_xH_{2x+2}. Here n represents the number of repeating units in the polyethylene chain.

Polymers can be divided in two categories based on their origin: *synthetic* and *natural*. Synthetic polymers are man-made polymers derived from petroleum oil. Examples of synthetic polymers include nylon, polyethylene, polyester, Teflon, and epoxy. Natural polymers occur in nature and are often water-based. Examples of naturally occurring polymers are silk, wool, DNA, cellulose and proteins.

Many natural polymers have been common at homes for centuries, but during the most recent decades synthetic polymers have replaced natural polymers in many appliances. Previously tools and containers were usually manufactured from materials such as wood, stone, iron or glass, but nowadays most of them are made of, at least partly, different plastics. The increased use and success of synthetic polymers have been based on economic factors such as advanced oil drilling techniques, and the fact that as natural materials become scarcer they become relatively more expensive [92].

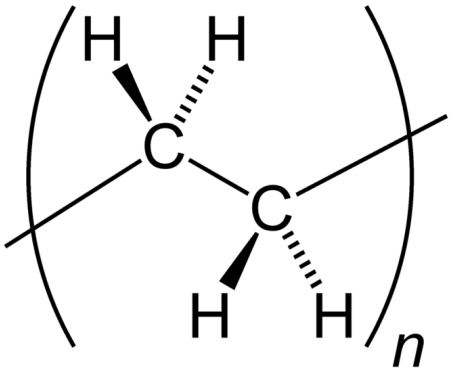

Figure 2: The repeating unit of polyethylene.

Another feature which can be used to categorize polymers is the degree of crystallinity. Polymers may be fully or partially crystalline, or completely disordered (amorphous). The disordered state may be glassy and brittle, molten and viscous or, it may be rubbery. In general, *branched* and *cross-linked* polymers tend to be amorphous while a linear polymer can be either amorphous or partly crystalline depending upon how it is manufactured.

Examples of branched and cross-linked polymers are shown in Figs. 3 and 4. In polymer chemistry, branching occurs by the replacement of a substituent, such as a hydrogen atom, on a monomer subunit, by another covalently bonded chain of that polymer. Branching interferes with the orderly packing of molecules, so that the degree of crystallinity decreases.

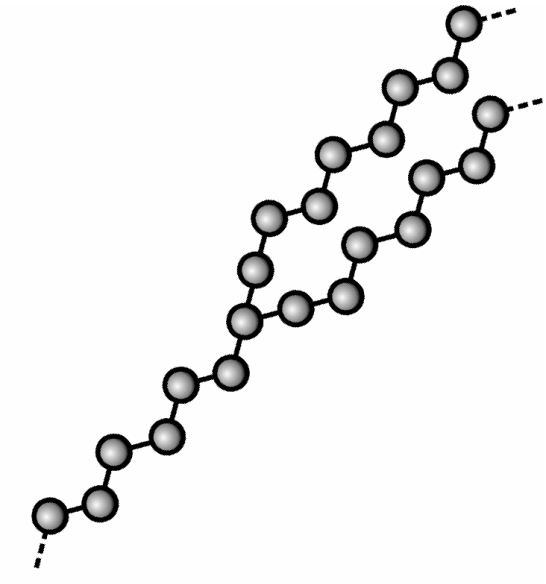

Figure 3: Branch point in a polymer. (Image source: Wikipedia article [95])

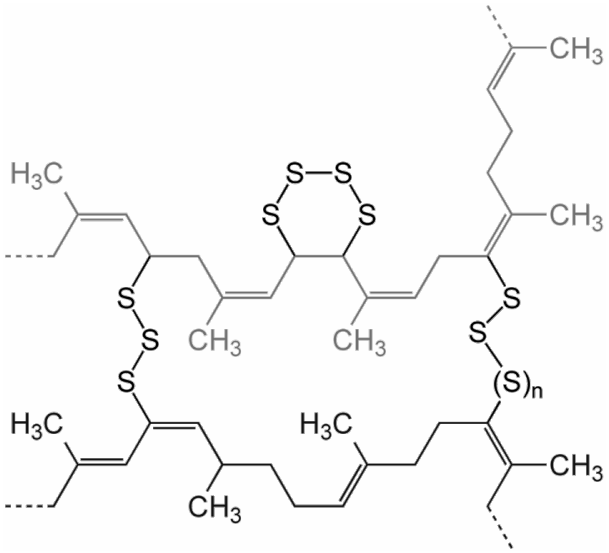

Figure 4: Vulcanization is an example of cross-linking. Two polyisoprene chains are cross-linked by added sulfur atoms. (Image source: Wikipedia article [96])

In cross-linking rubber by vulcanization, short sulfur branches link polyisoprene chains into a multiply branched *thermoset*[1] *elastomer*[2]. Rubber can also be so completely vulcanized that it becomes a rigid solid, so hard it can be used to make bowling balls. Branching sometimes occurs spontaneously during synthesis of polymers; e.g., in free-radical polymerization of ethylene to form polyethylene. In fact, preventing branching when producing linear polyethylene requires special methods.

The extent to which polymer molecules will crystallize depends on their structures and on the magnitudes of the secondary bond forces (van der Waals forces) among the polymer chains. The greater the linearity of the polymer molecule and the stronger the intermolecular forces, the greater the tendency toward crystallization. Linear PE has essentially the best structure of all polymers for chain packing. Its molecular structure is very simple and perfectly regular, and the small methylene groups fit easily into a crystal lattice. Linear HDPE therefore crystallizes easily and to a high degree (70-80%) even though its intermolecular forces are small [33].

[1]Polymeric material irreversibly hardened by cross-links into a rigid shape.
[2]A material with both elastic and viscous properties.

3.2 Polyethylene

Polyethylene is the most widely used plastic, with an annual production of approximately 80 million tons [70]. Structurally polyethylene is a thermoplastic[3] polymer consisting of long chains produced by combining the ingredient ethylene $CH_2{=}CH_2$. The ethylene repeat unit combines in long polyethylene chains shown in Fig. 5.

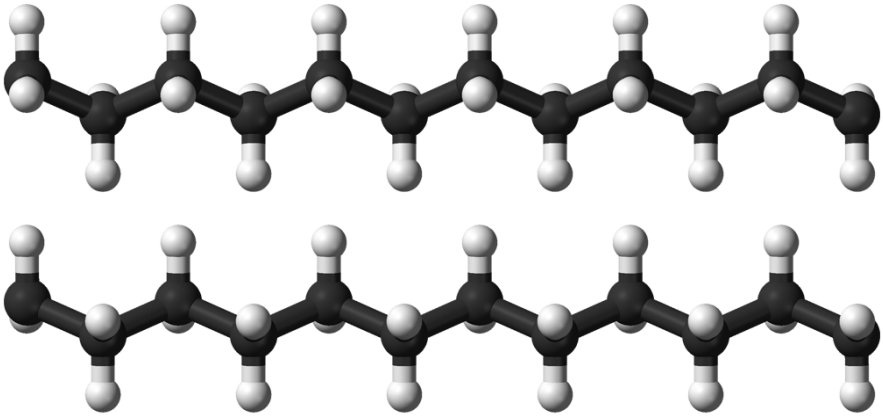

Figure 5: Polyethylene chains.

3.2.1 Types of polyethylene

Polyethylene is classified into several different categories based mostly on its density and branching. The mechanical properties of PE depend significantly on variables such as branching, cross-linking, crystallinity and the molecular weight.

The most common types of PE are *low-density polyethylene* (LDPE), *linear low-density polyethylene* (LLDPE), *cross-linked polyethylene* (PEX or XLPE), *high-density polyethylene* (HDPE), and *ultra-high-molecular-weight polyethylene* (UHMWPE). The HDPE is the subject of study in publications **I-IV** of this thesis. Table 1 compares some of the fundamental properties of these different PE types. With regard to industrial production, the most important polyethylene grades are HDPE, LLDPE and LDPE.

UHMWPE has an extremely high molecular weight with a molecular mass up to $6 \cdot 10^6$ g/mol [85] due its long polymer chains (up to 200000 ethylene units). The long chains make UHMWPE a very tough material, with the highest impact strength of any

[3] A polymer that becomes moldable above a specific temperature, and returns to a solid state upon cooling. [10]

thermoplastic presently made [85]. UHMWPE is used in many applications where extreme durability is needed, such as in hip and knee implants and in bulletproof vests.

PEX is a form of polyethylene with a large number of cross-linked bonds in the polymer structure, typically 65–89% of the chains are cross-linked, changing it from thermoplastic to a thermoset [18]. PEX is usually formed into tubing, and is used predominantly in industrial pipework systems, domestic water piping, and as insulation for high voltage electrical cables. Almost all PEX is made from HDPE.

Table 1: Typical values of crystallinity, density, melting point, tensile strenght and the average number of branches in different types of PE. Values adapted from [51] (UHMWPE), [33] (HDPE), [50] (LDPE and HDPE), [24] (LDPE and LLDPE), [18] (PEX),[79] (LLDPE) and [41] (all TS values).

Type of PE	Crystallinity %	Density g/cm^3	Melting Point °C	Tensile Strength MPa	# Branches per 1,000 C atoms
LDPE	35-50	0.91-0.94	105-116	10-20	10-40
LLDPE	65-80	0.92-0.94	125	10-35	4-21
PEX	30-50	0.92-0.94	133	15-30	10-25
HDPE	70-80	0.94-0.97	120-140	15-40	$<$ 5-10
UHMWPE	39-75	0.93-0.94	125-138	30-53	?

LDPE is defined by a density range of 0.910–0.940 g/cm^3 (see Table 1) and molecular weight of less than 50000 g/mol [51]. LDPE has a high degree of short and long chain branching, causing decreased ability for the chains to pack into a crystal structure. Thus it has weaker intermolecular forces and this results in a lower tensile strength and increased ductility. The high degree of branching with long chains gives molten LDPE unique and desirable flow properties. LDPE is used for both rigid containers and plastic film applications such as plastic bags and film wrap. In 2009 the global LDPE market had a volume of circa $22.2 billion [20].

LLDPE has a similar density range and molecular weight to LDPE. LLDPE is a very linear polymer with significant numbers of short branches to increase linearity [79]. LLDPE has a higher tensile strength than LDPE, and higher impact and puncture resistances. Because of this LLDPE can be made into films with lower thickness than those made of LDPE, and, with a better environmental stress resistance. LLDPE is mainly used in packaging, particularly film for bags and sheets. In 2009 the world LLDPE market volume was almost $24 billion [21].

The main subject in publications **I-IV** is high-density polyethylene. HDPE is defined by a density of greater than 0.94 g/cm^3 (shown in Table 1). HDPE has a low degree of branching and thus stronger intermolecular forces and tensile strength. It takes 1.75

kilograms of petroleum to make one kilogram of HDPE [54]. HDPE can be produced using chromium/silica catalysts, Ziegler-Natta catalysts or metallocene catalysts. The lack of branching is ensured by an appropriate choice of catalyst and reaction conditions. HDPE is widely used in products and as a packaging material. For example, one third of all toys are manufactured from HDPE [19]. In 2007 the global HDPE consumption reached a volume of more than 30 million tons [19].

The molecular structure of different types of PE explains some of the trends found in the data in Table 1. Branching impairs the regularity of the structure and hinders chain packing. Branched LDPE is thus only partially (35-50%) crystalline. On the other hand the lower crystallinity of UHMWPE is explained by its extreme molecular length which makes efficient chain packing difficult. Many of the differences in physical properties between low-density and high-density PE's can be attributed to the higher crystallinity of the latter. Thus, linear HDPE has higher density than the branched material (density range of 0.94-0.97 g/cm^3 vs 0.91-0.93 g/cm^3), higher melting point (typically higher than 125 °C compared to 112 °C), greater stiffness and tensile strength, greater hardness, and lower permeability to gases and vapours.

3.3 Cellulose

Cellulose $(C_6H_{10}O_5)_n$ is a natural polymer, a long chain of $\beta(1 \rightarrow 4)$ linked D-glucose molecules. It is the main component of plant cell walls, and the basic building block for many textiles and for paper. Cotton is the purest natural form of cellulose. In the laboratory, ashless filter paper is a source of nearly pure cellulose.

Most of the wood species contain 40-45% of cellulose [84]. Cellulose is mainly used to produce paperboard and paper. Cellulose fibers in wood are bound in lignin[4], and paper-making involves treating wood pulp with alkalis or bisulfites to disintegrate the lignin, and then pressing the pulp to matte the cellulose fibers together. Despite its great abundance, cellulosic biomass has seen limited application outside the paper industry. Its use as a feedstock for fuels and chemicals has been hindered by its highly crystalline structure, inaccessible morphology and limited solubility.

Even though cellulose is insoluble in water and most organic solvents, many cellulose derivatives, however, are non-crystalline and dissolve readily in organic solvents. Substituents in general decrease molecular chain stiffness and increase solubility and fusibility, the effect being greater the larger the substituents group.

[4]Lignin is a natural polymer binding the cells, fibres and vessels which constitute wood. After cellulose, it is the most abundant renewable carbon source on Earth.

3.3.1 General properties

Cellulose has no taste, is odourless, hydrophilic, chiral, biodegradable, and insoluble in water and most organic solvents. It can be broken down chemically into its glucose units by treating it with concentrated acids at high temperature. Cellulose has no melting point [80] (incineration occurs before plastification) and is fairly resistant to thermal degradation.

Structurally cellulose is an unbranched polymer of high molecular weight, its repeating unit consisting of two anhydroglucose rings (shown in Fig. 6). Many properties of cellulose depend on its chain length (degree of polymerization). Cellulose chains from wood pulp have typical chain lengths between 300 and 1700 glucose units; cotton and other plant fibers as well as bacterial cellulose have chain lengths ranging from 800 to 10000 units [47].

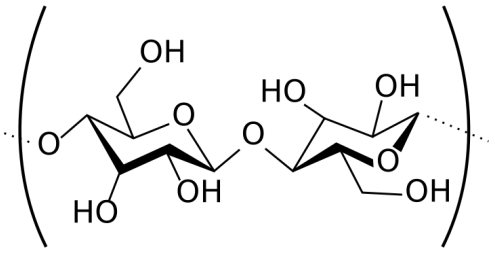

Figure 6: The repeating unit of cellulose.

The regular structure of the polymer allows crystal structures to be formed and according to X-ray measurements cellulose is 70-85 % crystalline [66]. This high degree of crystallinity is associated with hydrogen bond formation between adjacent chains, and these strong intermolecular forces are sufficient to permit considerable expansion of the unit cell without disruption during swelling by strong acids and alkalis [23].

3.3.2 Different crystal structures

Cellulose has been found to form several different crystalline structures, corresponding to different hydrogen bonding networks between and within cellulose chains. Natural cellulose is cellulose I, with structures Iα and Iβ [6]. Cellulose produced by bacteria and algae is enriched in Iα while cellulose of higher plants consists mainly of Iβ [39]. An orthographic view of the Iβ structure is shown in Fig. 7. The simulation system used to model cellulose in publications **I, IV** and **V** represents the Iβ structure taken from [100].

Later it has been discovered that the ultrastructure of natural cellulose possesses unexpected complexity as Iα and Iβ can be found not only within the same cellulose sample, but also along a given microfibril [60]. The relative amounts of Iα and Iβ vary between samples of different origins. Whereas Iα rich specimens have been found in the cell walls of some algae and in bacterial cellulose, Iβ rich specimens have been found in cotton, wood and ramie fibers [60]. In comparison to the Iα phase, the Iβ-phase has been found to be thermodynamically more stable [39].

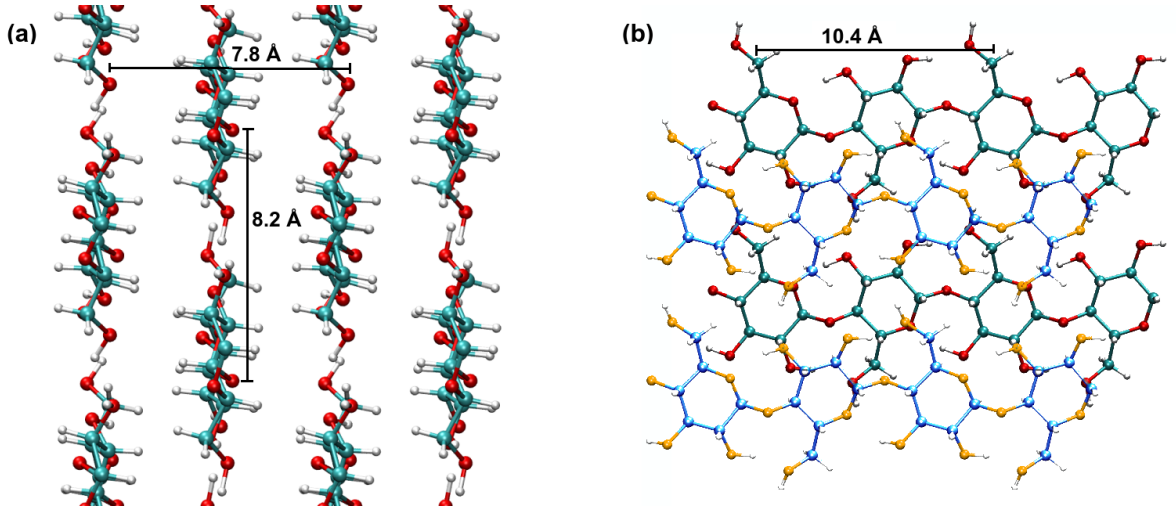

Figure 7: Cellulose Iβ crystal structure. **(a)** an orthographic view of the system along the chain direction. **(b)** a view along the axis perpendicular to chain direction and the plane of glucose rings. Hydrogen atoms are white, carbon blue and oxygen atoms red.

Cellulose in regenerated cellulose fibers is cellulose II [65]. It may be obtained from cellulose I by either of two processes: a) regeneration, which is the solubilization of cellulose I in a solvent followed by reprecipitation by dilution in water to give cellulose II, or b) mercerization, which is the process of swelling native fibres in concentrated sodium hydroxide, to yield cellulose II on removal of the swelling agent. The conversion of cellulose I to cellulose II is irreversible, suggesting that cellulose I is metastable and cellulose II is stable [48].

With various chemical treatments it is possible to produce the structures cellulose III and cellulose IV: Celluloses III_I and III_{II} are formed, in a reversible process, from celluloses I and II, respectively, by treatment with liquid ammonia or some amines, and the subsequent evaporation of excess ammonia. Polymorphs IV_I and IV_{II} may be prepared by heating celluloses III_I and III_{II} respectively, to 206 °C, in glycerol [65].

4 LOW-ENERGY RADIATION EFFECTS IN SOLIDS

4.1 Overview

Radiation can be defined as the propagation of energy through matter or space. It can be in the form of electromagnetic waves or energetic particles. Radiation originates both from natural sources such as sunlight or lightning discharges, and man-made sources such as accelerators (ions, electrons), reactors (neutrons), wireless communications, and medical applications.

Radiation can be divided into two categories based on its effect on the target material. *Non-ionizing radiation* does not have enough energy to ionize atoms in the material it interacts with. Forms of non-ionizing radiation include microwaves, radio waves, visible light and ultraviolet radiation (except for the very shortest wavelengths). *Ionizing radiation*, on the other hand, has enough energy to knock electrons from an atom, i.e. to ionize. Ionizing radiation comes in the form of ion beams, α or β particles, neutrons, X-rays and γ radiation.

The five basic mechanisms of any energy interchange between ionizing radiation and atoms of the target sample are [23]:

1. Ionization - a process in which an orbital electron is removed from its parent nucleus giving rise to a free electron and a positively charged (ionized) atom or molecule. Ionization is not a relevant effect in metals but it has important consequences in organic materials, e.g. the DNA in living cells can be damaged by ionization causing an increased chance of cancer [4]. Unfortunately ionization is not tractable by the simulation method used in this thesis.

2. Excitation - in which an electron is raised to a high energy level but remains bound to its parent nucleus. In this case, the atom or molecule remains neutral. The excitation phenomenon is also outside the scope of this thesis.

3. Displacement of a nucleus with or without its attendant electron.

4. Capture of the incident particle by an atomic nucleus and transformation of the nuclear structure.

5. Scattering of the incident particle or photon and emission of secondary radiation.

When the recoil energy given to the target atom is larger than the *damage threshold energy* (DTE), the radiation produces damage of types 3–5.

The DTE is the minimum kinetic energy that an atom in a solid needs to be permanently displaced from its lattice site to a defect position. It is quite commonly known as 'displacement threshold energy', but in this thesis the word *damage* is used instead of *displacement* since in organic materials damage can occur in form of broken bonds without atoms being 'displaced'. In a crystal, a separate threshold energy exists for each crystallographic direction and one should distinguish between the minimum DTE $\equiv$ DTE_{min} and the average DTE $\equiv$ DTE_{ave} calculated over all lattice directions[5]. Average DTEs in typical solids are of the order of 20–50 eV [5]. As will be demonstrated by our DTE results for HDPE and cellulose in Section 6.1, for organic polymers the situation is even more complex as each atom in the monomer typically has a different DTE from other atoms and a strong directional dependence related to the local bonding structure.

In this thesis we concentrate on studying ionizing radiation with recoil energies close to and above the DTE, corresponding to recoil energies caused by e.g., electron beams, neutrons or ions with $E_{kin} \ll 1$ MeV. One reason for limiting high-energy recoils outside the scope of this study comes from the simulation setup: computational costs dictate that the simulated material sample is only a few nm in diameter, with periodic boundary conditions, and thus the energy given to the recoil atom should not be so large that the recoil kicks the atom over the periodic boundaries (doing so might cause unphysical self-interaction effects).

The upper limit for the maximum recoil energy our simulation system can contain is roughly 100–500 eV, depending strongly on the recoil direction. In a binary collision between the incoming irradiation particle (mass m) and an atom in the target sample (mass M), the maximum energy T_{max} that an incident particle can transfer to the target is given by the formula [102]

$$T_{max} = \frac{2ME(E + mc^2)}{(M+m)^2c^2 + 2ME} \approx \frac{4EMm}{(M+m)^2}, \tag{1}$$

where E is the kinetic energy of the incoming particle, and the approximation is valid if $E \ll mc^2$. If the irradiating particle is a proton, the maximum recoil energy for a C atom in the target sample is $0.28 \times E_{kin}$ and for an O atom $0.22 \times E_{kin}$. For electrons, it also follows from Eq. 1 that $T_{max} \approx 2 \cdot 10^{-4} \times E_{kin}$ for H atoms and $2 \cdot 10^{-5} \times E_{kin}$ for C atoms. Thus the maximum energy transfer from e.g. a 100 keV electron to C atom in target sample is 20 eV, and to a H atom 220 eV. With a 500 keV electron energy, T_{max} to a H atom rises already to 1.6 keV, and to a C atom T_{max} is 136 eV.

The other reason for modelling relatively low energies is that for ion irradiation *electronic stopping* starts to dominate over *nuclear stopping* when the energy of the incoming ion $E_{inc} \gtrsim 0.1$ MeV, and our simulation model does not include electronic effects.

[5]From now on, the subscript will be omitted for average DTE, meaning DTE $\equiv$ DTE_{ave}.

4.2 Electronic and nuclear stopping

The slowing down of an incoming ion, due to inelastic collisions with bound electrons in the medium, is called electronic stopping. Since the number of collisions an ion experiences with electrons is large, and since the charge state of the ion while traversing the medium may change frequently, it is very difficult to describe all possible interactions for all possible ion charge states. Thus the electronic stopping power is usually given as a simple function of energy $S_e(E)$ [81].

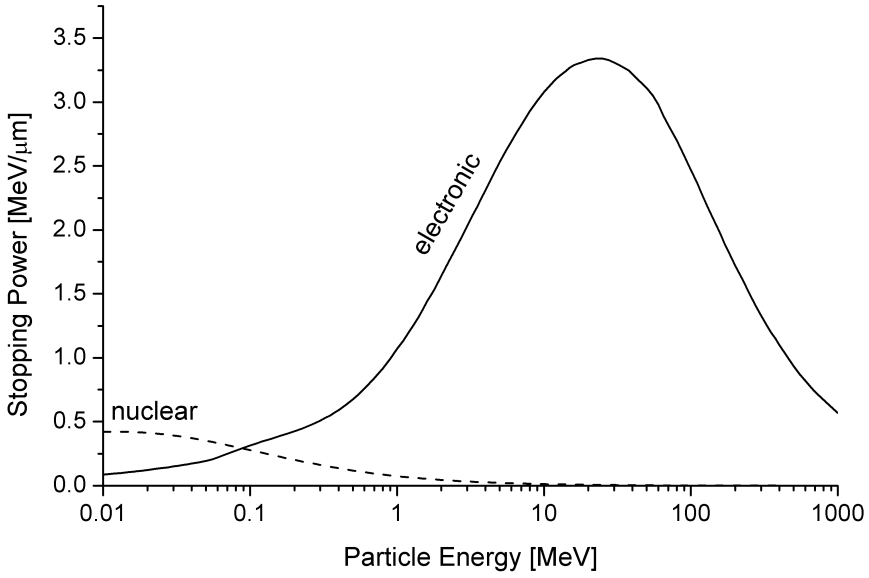

Figure 8: Electronic stopping and nuclear stopping for aluminium ions in aluminium.

By nuclear stopping, one refers to elastic collisions between the ion and atomic nuclei in the sample. Figure 8 shows electronic and nuclear stopping power for aluminium ions in aluminium, versus particle energy per nucleon. The maximum of the nuclear stopping curve typically occurs at energies of the order of 1 keV per nucleon [68].

If the repulsive potential $V(r)$ between two interacting atoms is known, it is possible to calculate the nuclear stopping power $S_n(E)$. As can be seen from Fig. 8, electronic stopping starts to dominate over nuclear stopping when the energy per nucleon $\gtrsim 0.1$ MeV. Nuclear stopping increases when the mass of the ion increases, and for very light ions slowing down in heavy materials, the nuclear stopping is weaker than the electronic stopping at all energies.

At energies between 0.01 and 1.0 MeV, the stopping power is the sum of two terms:

$S(E) = S_e(E) + S_n(E)$. Several semi-empirical stopping power formulas have been devised. The model given by Ziegler, Biersack and Littmark [102] (the so called "ZBL" stopping) implemented in the SRIM code [101], was used in Publication **II** in this thesis.

4.3 Radiation effects in polymers

The irradiation of polymeric materials with ionizing radiation (gamma rays, X-rays, accelerated electrons, ion beams) leads to the formation of very reactive intermediates, free radicals, ions and excited states [25]. Nowadays, the modification of polymers covers radiation induced polymerization (*graft polymerization*[6]), the degradation of polymers (*chain scission*) and radiation cross-linking.

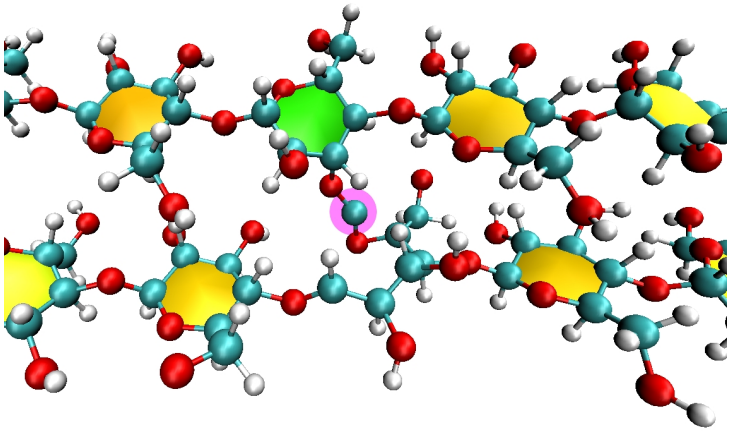

Figure 9: A cross-link between two polymer chains in cellulose.

Chain-scissioning can be achieved, for example, through electron beam (EB) processing. EB processing can cause the degradation of polymers, breaking chains and therefore reducing the molecular weight. An example of this process is the breaking down of cellulose fibers extracted from wood in order to shorten the molecules, thereby producing a raw material that can be used to produce biodegradable detergents and diet-food substitutes.

Cross-linking of a polymer means that on the atomistic scale the polymer chains are connected to each other by covalent or ionic bonds. A cross-link in cellulose is shown in Fig. 9. When matter is cross-linked, its physical properties change: typically the relative motion of polymer chains, the creep rate, decreases and dimensional stability is improved. This affects the strength, causing rubber-like elasticity. In fact, without cross-links this kind of elasticity would not generally occur [1]. It has also been observed that

[6] A graft polymer molecule is a branched polymer molecule in which one or more of the side chains are different, structurally or configurationally, from the main chain.

the thermal resistance (resistance against heat distortion) increases with the increasing cross-link density of the material (Cowie [27], p. 346).

Cross-linking can be carried out by irradiating with high energy electrons, ions or rays. Typical dose requirements for cross-linking are in the range of 50-200 kGy [26]. Alternatively, cross-linking can be achieved by chemical processes that are initiated by heat, pressure and another substance which contains the so-called cross-linking reagents. The prominent drawbacks of chemical cross-linking typically involve the generation of noxious fumes and by-products of peroxide degradation [25]. In this thesis the focus of study will be on irradiation induced cross-linking.

4.3.1 Polyethylene and irradiation

The most typical effects seen in a polyethylene sample after irradiation are chain-scissioning (broken chains), radical formation and cross-linking. A broken PE chain is shown in Fig. 10. Cross-linking is the most important of these reactions from applications' point of view.

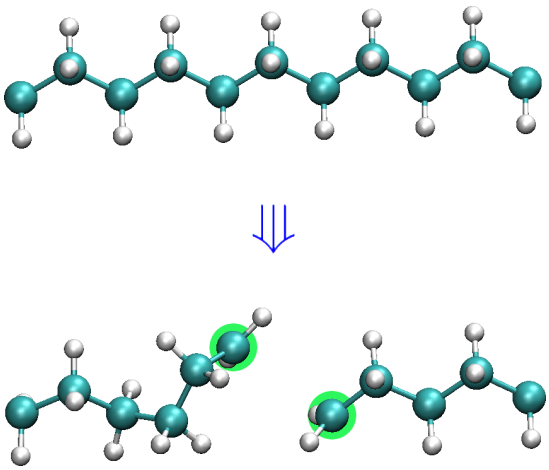

Figure 10: A broken polymer chain in PE.

Radiation cross-linked polyethylene is a basic material used in many wire and cable insulations. It is also used in heat shrinkable tubes and tapes, for piping and for warm water supply, for foamed materials and for mould parts (end caps, electronic components, machinery and automotive parts, etc.) [34].

The radiation doses required for cross-linking in pure LDPE or HDPE samples are much higher than, for instance, the ones needed for PE samples diluted in aqueous solutions [83]. Experiments have also shown that, in general, cross-linking in LDPE is easier to achieve than in HDPE, because of a greater fraction of an amorphous phase [83]. It has been claimed that the length of the carbon-carbon bond is too short (ca. 1.54 Å) for crosslinking of adjacent chains in the crystal lattice of pure HDPE where the relative distance of chains is near to 4.1 Å [67].

It is widely accepted that free-radical reactions contribute to PE cross-linking [34], though opinions on the precise details and the types of free radicals involved vary [82]. The details of cross-link formation in pure, crystalline HDPE are studied in publications **I** and **II** of this thesis.

4.3.2 Cellulose and irradiation

Figure 11 shows three typical damage types occurring in cellulose after a recoil event. In the top panel radical formation is demonstrated, in the middle panel a broken glucose ring, and in the bottom panel chain scission.

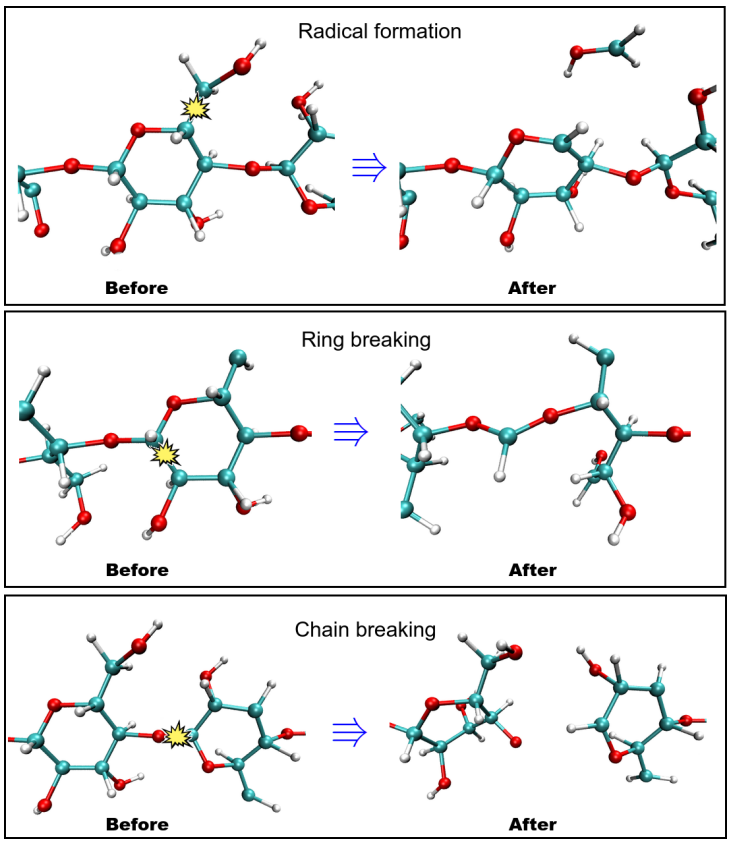

Figure 11: Image sequence showing the three typical damage types occuring in cellulose as results of a recoil event.

Even though irradiation processing techniques have been widely and successfully applied to synthetic polymers for decades, the natural polymers have been found to be difficult to process, and to suffer main chain degradation and other chemical changes of less well defined character, when exposed to high-energy radiation [25]. In recent years, natural polymers are being looked at again with renewed interest because of their unique characteristics such as inherent renewability, biocompatibility, biodegradability and easy availability. Irradiation has long been discussed as a means of modifying cellulose for different purposes, such as better processability in subsequent production stages or the transformation to low molar mass products in the context of chemical generation from woody biomass [40].

The effects of EB radiation and γ irradiation on cellulose have been evaluated in a multitude of studies. In general, ionizing radiation causes degradation of cellulose. The degradation of various types of cellulose pulps and papers by EB irradiation has been noted in various recent studies [42, 15, 29]. On the other hand, it has been reported that EB treatment can improve some properties of microcrystalline cellulose with regard to food application [58] and that such irradiation enhances acidic hydrolysis of bagasse[7] more than enzymatic hydrolysis. In the case of γ irradiation, studies agree that different cellulose and paper grade pulps decrease their molar mass while the oxidized cellulose functionalities are increased [88, 98]. However, at γ radiation doses below 15 kGy, no impact on paper stability was found by mechanical tests [31].

The effects of irradiation with recoil energies from 5 to 100 eV in crystalline cellulose Iβ samples are studied in publications **I** and **V** of this thesis.

[7]Bagasse is the fibrous matter that remains after sugarcane or sorghum stalks are crushed to extract their juice.

5 COMPUTATIONAL METHODS

In this section, the computer simulation methods that have been used in this work are described. The concept of molecular dynamics is explained and the inter-atomic potentials required for the simulations are detailed. The specific features of each potential and approaches that are especially important for irradiation simulations are also described.

5.1 Molecular dynamics

Molecular dynamics (MD) is a simulation method based on solving classical equations of motion for a system consisting of many interacting objects, quite often atoms. MD was first used in the 1950's [2], and since then its popularity has been increasing constantly, thanks to the ever-growing computational power. In MD simulations the computational time often scales linearly with the number of atoms in the simulation, so if one can simulate a small system for 10 ns, then a system with ten times more atoms can be simulated only for 1 ns. In the earliest MD simulations the number of particles was about 1000, and the system could be simulated for a few picoseconds (1×10^{-12} s) [77]. Today's computational resources allow us to model systems as big as 100 million particles for several nanoseconds.

5.1.1 Simulation algorithms

Figure 12 describes the iteration algorithm behind a typical atomistic MD simulation procedure. Starting with initial positions $\mathbf{r}_i$ and velocities $\mathbf{v}_i$ of the atoms $i = 1 \ldots N$, and given an inter-atomic potential $V(\mathbf{r}^N)$, the force acting on each atom is derived from

$$\mathbf{F}_i = -\nabla_{\mathbf{r}_i} V(\mathbf{r}^N), \text{ where } \mathbf{r}^N = (\mathbf{r}_1, \mathbf{r}_2, \ldots \mathbf{r}_N), \tag{2}$$

and then the equations of motion,

$$m_i \mathbf{a}_i = m_i \frac{\partial^2 \mathbf{r}_i}{\partial t^2} = \mathbf{F}_i, \tag{3}$$

are integrated over a small time step Δt. Here m_i and $\mathbf{a}_i$ are the mass and acceleration of atom i.

The integration is done numerically by using a suitable efficient integrator algorithm. The Gear 5 predictor-corrector algorithm [3] is employed in the MD code PARCAS [62] which was used in this thesis in all the simulations involving HDPE. With Gear 5, the numerical errors cause very small energy fluctuations, but they are not reversible, so there is always a small drift in the total energy of the simulation system. In the simulation

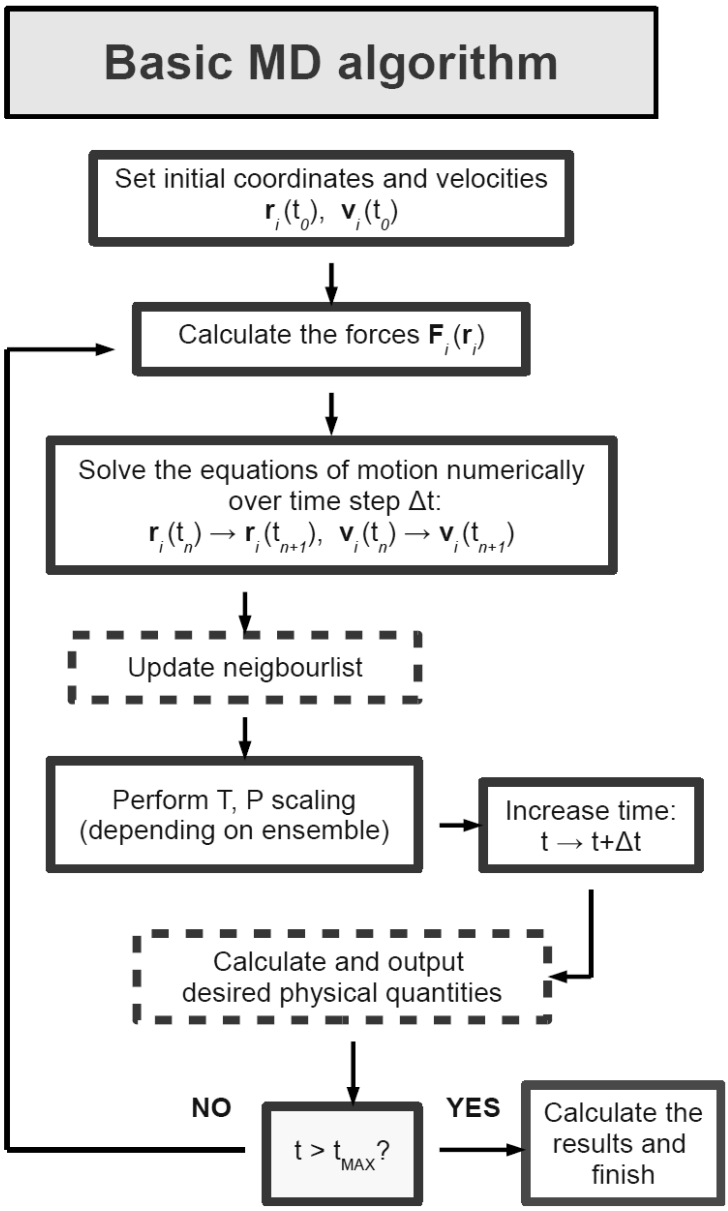

Figure 12: Flowchart of a simple MD algorithm.

code used to model cellulose irradiation, the Velocity Verlet [87] integration algorithm was used. Compared to Gear 5, Velocity Verlet is computationally more simple, and has bigger energy fluctuations, but the total energy of the system is stable, assuming an appropriate time step value is used.

The choice of the time step Δt is crucial in ensuring the conservation of energy in MD simulations; if it is too long, energy is not conserved, if too short, the computational time is increased unnecessarily. Therefore, an adaptive time step was used in all the simulations performed in this thesis. This means that whenever energetic particles are present in the simulation system, Δt becomes shorter, and as the system cools down and the kinetic energy of energetic atoms is transformed into potential energy, the time step is gradually increased. In the simulations of this thesis, typical values of Δt are 0.1–0.2 fs.

After new positions and velocities are acquired, it might be necessary to update the neighbour list[8] (see the flowchart in Fig. 12). Usually it is enough to do this once in every 10 simulation steps or so.

The temperature control in the simulations performed in this thesis was done using the method developed by Berendsen et al. [13]. Here the system temperature T is controlled by coupling it to an external heat bath of desired temperature T_0. This can be achieved by adding a friction term into the equations of motion (Eq. 3), yielding

$$m_i \mathbf{a}_i = \mathbf{F}_i + m_i \gamma (\frac{T_0}{T} - 1) v_i, \tag{4}$$

where v_i is the velocity of particle i and γ is the damping constant.

Since the temperature of the system is defined by the velocities of the atoms in it, the temperature control can also be achieved by scaling the velocities at every time step Δt. With the Berendsen thermostat the multiplication factor is

$$\lambda = \sqrt{1 + \frac{\Delta t}{\tau_T} (\frac{T_0}{T} - 1)}, \tag{5}$$

where $\tau_T = \frac{1}{2\gamma}$ is the time constant determining the scaling rate. The Berendsen pressure control [13] was used to control the pressure of the system in the relaxation simulations performed in publications **I** and **II**.

After the T and P control phase in the MD algorithm, the simulation program might output some desired physical quantities (e.g. simulation time, atom coordinates, T, E_{kin}, E_{pot}, etc.). Then the algorithm checks if the simulation time exceeds the given maximum time; if not, the algorithm returns back to the force calculation phase, and if yes, the program ends.

5.1.2 Inter-atomic potentials

Computationally the most demanding and time consuming part of the MD simulation algorithm is the calculation of forces (see Eq. 2) from the inter-atomic potential $V(\mathbf{r}^N)$. In

[8] A list of nearby atoms for each atom in the system. Of all atoms, only those on the atom's neighbour list are taken into account in the force calculation, and the effect of other atoms in the system is considered to be negligible.

this thesis two different potential models were used, both based on the reactive empirical bond order (REBO) potential by Brenner [16].

AIREBO

In the simulations involving polyethylene, the inter-atomic interactions were modelled with AIREBO [86, 17], a reactive potential for hydrocarbons with intermolecular interactions. The potential has the form

$$E = \frac{1}{2}\sum_i \sum_{j\neq i} \left[E_{ij}^{\mathrm{REBO}} + E_{ij}^{\mathrm{LJ}} + \sum_{k\neq i,j} E_{kijl}^{\mathrm{tors}} \right], \tag{6}$$

where the three terms correspond to covalent forces between atoms, van der Waals interactions between molecules and torsional interactions, respectively.

The covalent part of the potential is based on the form proposed by Tersoff [89],

$$E_{ij}^{\mathrm{REBO}} = V_{ij}^{\mathrm{R}} - b_{ij} V_{ij}^{\mathrm{A}} \tag{7}$$

where the repulsive (V^{R}) and attractive (V^{A}) contributions are combined in a ratio determined by the bond-order term b_{ij}.

The pairwise interaction terms in Eq. 7 have functional forms as follows:

$$V_{ij}^{\mathrm{R}}(r) = \quad w_{ij}(r_{ij}) \left[1 + \frac{Q_{ij}}{r_{ij}} \right] A_{ij} e^{-\alpha_{ij} r_{ij}} \tag{8}$$

$$V_{ij}^{\mathrm{A}}(r) = \quad -w_{ij}(r_{ij}) \sum_{n=1,3} B_{ij}^{(n)} e^{-\beta_{ij}^{(n)} r_{ij}} \tag{9}$$

where the parameters Q_{ij}, A_{ij}, $B_{ij}^{(n)}$, α_{ij}, and $\beta_{ij}^{(n)}$ depend on the atom types i and j. Values for these are given in Table II of Ref. [86]. The w_{ij} term is a bond weighting factor,

$$w_{ij}(r_{ij}) = S'(t_c(r_{ij})), \tag{10}$$

that switches off the REBO interactions when the atom pairs exceed typical bonding distances. The functional forms of the switching function S' and the scaling function t_c are given in the Appendix of Ref. [86].

The b_{ij} term in Eq. 7 specifies the *bond order* for the interactions between atoms i and j,

$$b_{ij} = \frac{1}{2}[p_{ij}^{\sigma\pi} + p_{ji}^{\sigma\pi}] + \pi_{ij}^{\mathrm{rc}} + \pi_{ij}^{\mathrm{dh}}. \tag{11}$$

The function of this term is to modify the strength of a bond due to changes in the local environment. The π_{ij}^{rc} term depends on whether a bond between atoms i and j has radical

character and is part of a conjugated system, while π_{ij}^{dh} depends on the dihedral angle for the double bonds [17].

The principal contribution to b_{ij} comes from the covalent bond interaction, given by terms $p_{ij}^{\sigma\pi}$ and $p_{ji}^{\sigma\pi}$:

$$p_{ij}^{\sigma\pi} = \left[1 + \sum_{k\neq i,j} w_{ik}(r_{ik}) g_i(\cos\theta_{jik}) e^{\lambda_{jik}} + P_{ij}(N_i^{\mathrm{C}}, N_i^{\mathrm{H}})\right]^{-\frac{1}{2}}. \tag{12}$$

Here the penalty function g_i imposes a cost on bonds that are too close to one another, θ_{jik} being the bond angle from atom i to atoms j and k. The exact form of the small correction factor $e^{\lambda_{jik}}$ can be found in the Appendix of Ref. [86].

The last term in Eq. 12, function P_{ij}, represents a bicubic spline and the quantities N_i^{C} and N_i^{H} are the number of carbon and hydrogen atoms, respectively, that are neighbours of atom i.

The addition of van der Waals interactions, E_{ij}^{LJ}, and torsion interactions, E_{kijl}^{tors} is what differentiates AIREBO from the original REBO potential. Shortly,

$$E_{ij}^{\mathrm{LJ}} = C(r_{ij}) V_{ij}^{\mathrm{LJ}}, \tag{13}$$

where $C(r_{ij})$ contains several sets of switching functions similar to $S'(t)$ mentioned earlier[9], and

$$V_{ij}^{\mathrm{LJ}}(r_{ij}) = 4\varepsilon_{ij}\left[\left(\frac{\sigma_{ij}}{r_{ij}}\right)^{12} - \left(\frac{\sigma_{ij}}{r_{ij}}\right)^{6}\right], \tag{14}$$

is the traditional Lennard-Jones term. The torsional potential for the dihedral angle determined by atoms i, j, k and l, has a form

$$E_{kijl}^{\mathrm{tors}} = w_{ki} w_{ij} w_{jl} V^{\mathrm{tors}}(\omega_{kijl}), \tag{15}$$

where

$$V^{\mathrm{tors}}(\omega_{kijl}) = \frac{256}{405}\varepsilon_{kijl}\cos^{10}\left(\frac{\omega_{kijl}}{2}\right) - \frac{1}{10}\varepsilon_{kijl}. \tag{16}$$

REBO-CHO

In simulations involving cellulose, the REBO-CHO [59, 44] potential was used. REBO-CHO is based on the second generation REBO potential [17] which was parameterized to include oxygen-hydrocarbon interactions by Ni et al. [59], and later modified by Kemper and Sinnott [44].

[9]The exact form can be found from Ref. [86].

The REBO-CHO potential has the same functional form as the covalent interaction part of AIREBO (Eq. 7). The only difference to the equations presented above appears in Eq. 12:

$$p_{ij}^{\sigma\pi} = \left[1 + \sum_{k \neq i,j} w_{ik}(r_{ik}) g_i(\cos\theta_{jik}) e^{\lambda_{jik}} + P_{ij}(N_i^{\mathrm{C}}, N_i^{\mathrm{H}}, N_i^{\mathrm{O}})\right]^{-\frac{1}{2}}, \tag{17}$$

where the new argument N_i^{O} represents the number of O atoms that are neighbours of atom i [17].

The strategy used by Ni et al. in Ref. [59] for parametrization of the extended potential was the same as that taken by Brenner for pure hydrocarbon systems [16, 17]. First, they obtained the sets of parameters Q_{ij}, A_{ij}, B_{ij}, α_{ij}, and β_{ij}, for the repulsive and attractive terms of the potential that involve O. The parameters are developed so that the potential correctly reproduces a range of equilibrium distances and the bond energies for various O–O, C–O, and O–H bonds. The second phase of tuning the potential energies for specific molecules involves the parametrization of the bond order term, b_{ij}, according to the specific environment of each atom connected by the bond.

Unlike the approach taken by Brenner, however, the extended C–O, O–O, and O–H potential functions were fitted to values obtained exclusively by high-level, quantum chemical calculations rather than experimental bond energies and force constant values. A complete list of the parameter values, the calculated minimum energy values for bond energies and bond-lengths of representative molecules, and available experimental values are given in Table 1 of Ref. [59].

The published version of REBO-CHO potential does not include van der Waals forces or torsional interactions, but the simulation code[10] used in our simulations of cellulose included a standard Lennard-Jones potential (Eq. 14) for intermolecular interactions.

5.2 Simulation set-up

The set-up and analysis of all the simulations performed in this thesis are explained in more detail in the corresponding publications. Here the settings and procedures used for the simulations presented in the next section are briefly described.

Often irradiation of materials is simulated as a bombardment by a high energy particle, like an argon ion or a deuteron, on the surface of the specimen. For example in the work of Beardmore et al. [11], HDPE was bombarded by argon atoms with an energy of 1 keV. Another way to simulate the interaction between, e.g., the colliding electron and the lattice atom is by giving an initial kinetic energy, the recoil energy, to some

[10] Written mostly by Travis Kemper, further modified by the author with an adaptive time step and a new temperature control scheme.

randomly chosen atom (recoil atom) in the lattice. This method was used in this work. The direction of each collision, i.e. the direction of the initial velocity, was also generated randomly. This approach is suitable when one is not interested in sputtering or damage occurring at the surface, and when the concentration of ions in the specimen is small enough not to have a notable effect on the chemistry of the material.

In all irradiation simulations, the target crystal was relaxed at 0 K before the recoil event. Periodic boundary conditions were used in all directions. During irradiation, Berendsen temperature control [13] was applied at the cell borders (thickness 3 Å), to scale the temperature there towards 0 K.

In *damage threshold simulations*, the threshold energies for damage production in HDPE and cellulose were determined by giving the target atom a recoil energy in a random direction. Using a binary search algorithm, the recoil energy was tuned until the threshold energy for creating damage in the sample was pinpointed by 0.5 eV precision. The definition for the word *damage* used here is that at least one bond in the target sample is broken as a consequence of the recoil event. This process was then repeated 500 times for all targets to get a good coverage of all incident angles. Each of these simulations were run for 3 ps. In the damage threshold simulations for cellulose, the damage affecting only H atoms was ignored, to simplify the interpretation of the damage threshold maps, since H damage would be invisible in experiments such as TEM imaging.

All damage threshold maps presented in this thesis are based on 500 recoil events with a random initial recoil direction. Using these 500 data points as base values, the map grid is filled with interpolated values, of which the final map is composed. Note that when spherical maps are stretched to planar maps, the polar regions in the images are strongly elongated in the horizontal direction. The white bands in the top and bottom of the maps are caused by the insufficient number of data points occurring in the pole regions due to their small solid angle.

In the *single impact simulations* performed in publications **I** and **II**, 100 irradiation events were modelled with recoil energies of 5–100 eV. After a recoil event, HDPE simulations were run for 10 ps and cellulose simulations for 20 ps, to give the system some time to relax, and also to give all the reactions of interest enough time to occur. In the cellulose simulations of publication **I** hydrogen recoils were not modelled, since the H recoils had a high tendency to escape the periodic boundaries of the simulation box. For later publications the simulation procedure was improved to allow also H recoils with higher energies[11].

[11] In the simulations of publication **I** the recoil atom was always at the center of the system, thus allowing it to move by, at maximum, $\frac{1}{2}\times$ the longest box dimension before reaching the box boundaries. Later this was improved by moving the system in such a way that the recoil atom was positioned close to the borders of the system in the direction opposite to the recoil direction, thus maximizing the distance to the closest boundary in the recoil direction.

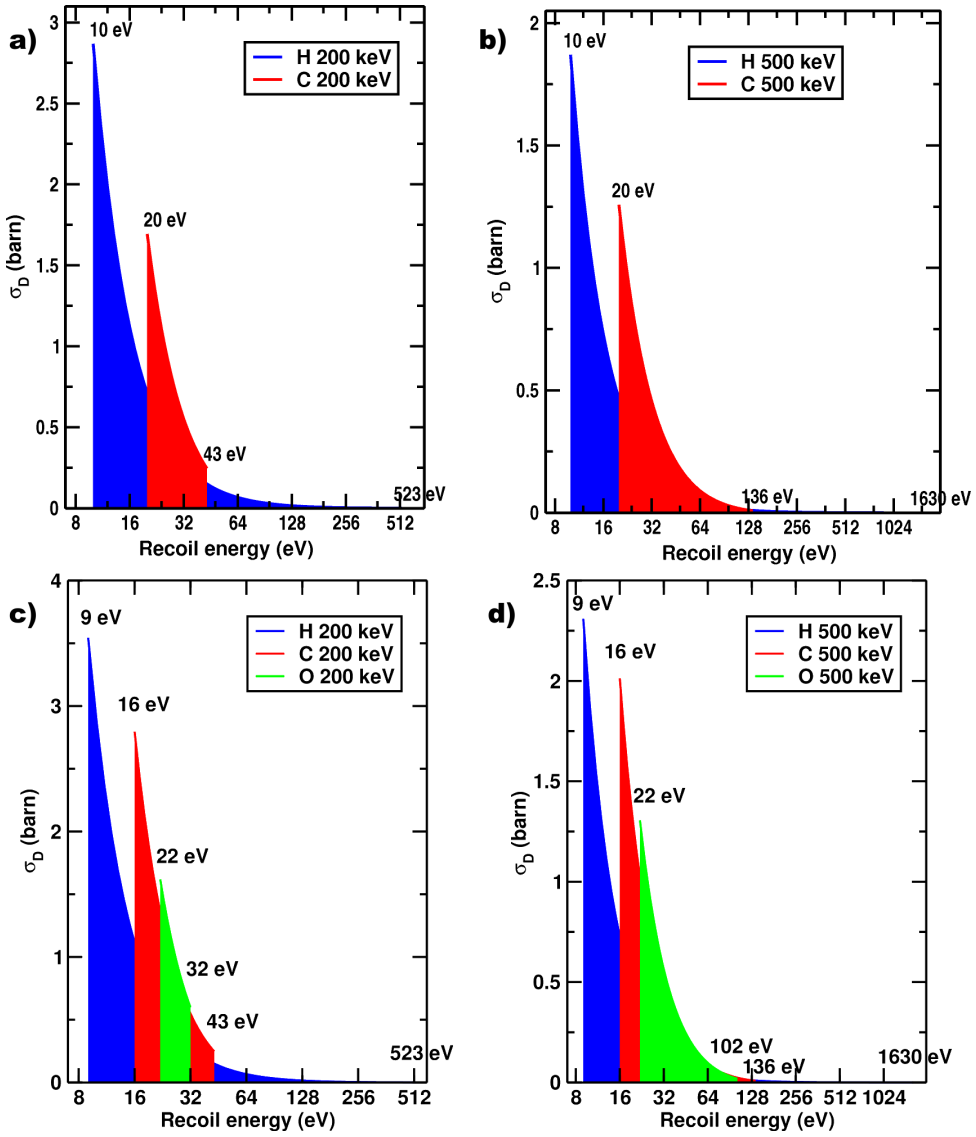

Figure 13: Threshold cross-section of hydrogen (blue), carbon (red) and oxygen (green) as a function of recoil energy for 200 keV (left plot) and 500 keV (right plot) electron irradiation. Distributions **a** and **b**, correspond to recoil atoms in HDPE, and distributions **c** and **d** to recoil atoms in cellulose.

In the *cumulative bombardment simulations* performed in publications **II** and **V**, electron irradiation was modelled with electron energies of 200 and 500 keV. In order to achieve a realistic recoil energy distribution for these simulations, the distribution of threshold cross-section σ_D as a function of energy was calculated using a form of the McKinley

Feshbach approximation [56] given by Lucasson [53],

$$\frac{\mathrm{d}\sigma}{\mathrm{d}T} = (2.5 \cdot 10^{-25}\mathrm{cm}^2)Z^2 \frac{1-\beta^2}{\beta^4}\frac{T_{max}}{T^2}\left[1 - \beta^2\frac{T}{T_{max}} + \pi\alpha\beta\left(\sqrt{\frac{T}{T_{max}}} - \frac{T}{T_{max}}\right)\right]. \quad (18)$$

Here T is the recoil energy, T_{max} the maximum energy transfer from electron to recoil atom (calculated using Eq. 1 on page 14), Z the atomic number, $\alpha \approx \frac{Z}{137}$ and $\beta = \frac{v_e}{c}$, the electron velocity divided by the speed of light. Calculations using Eq. 18 yielded the distributions shown in Figure 13.

To determine the relative amounts of different recoil types, the threshold cross-section was integrated over the recoil energy range,

$$\sigma_D = \int_{T_d}^{T_{max}} \Theta(T - T_d)\,\mathrm{d}\sigma(T). \quad (19)$$

Here T_d is the threshold energy for the onset of damage, acquired from damage threshold simulations, and $\Theta(T - T_d)$ is a simple step function. Using the integrated cross-section values, and taking into account the relative quatities of different atom types in polyethylene and cellulose, gave us the ratios for the different recoil atom types shown in Table 5.2.

Table 2: Relative amounts of different recoil atom types in cumulative bombardment simulations for HDPE and cellulose.

electron energy	H in HDPE	C in HDPE	H in cellulose	C in cellulose	O in cellulose
200 keV	77%	23%	60%	29%	11%
500 keV	67%	33%	46%	33%	21%

For both HDPE and cellulose samples, 20 sets of cumulative bombardment simulations were carried out using electron energies of 200 and 500 keV. The simulation time ranged from 3 to 10 ps depending on the recoil atom type and energy. Between each recoil event, the system was relaxed and cooled down with the Berendsen temperature control applied to all atoms; and in HDPE simulations, including Berendsen pressure control, with a time constant of 200 fs.

To obtain information about the size distribution of free radicals and broken polymer chains, we used a clustering algorithm developed in our group, where the atoms were grouped to fragments based on a cut-off distance, which takes into account the bond lengths between different atom types and periodic boundary conditions.

6 RESULTS

6.1 Threshold energy for damage production

In this section the main results from the threshold energy simulations are presented and some comparisons between HDPE and cellulose results are made.

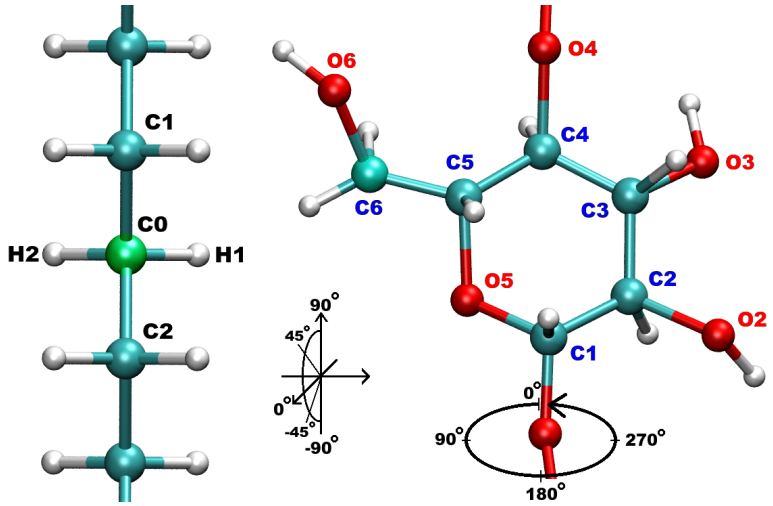

Figure 14: A visualization of the target molecules for the damage threshold simulations and the orientation of the recoil atoms.

Figure 14 shows the recoiling atoms for all damage threshold simulations. The left side of the image shows the PE chain with the recoil atoms C0 and H1 marked, as well as their nearest neighbouring atoms. The right side of Fig. 14 displays the recoil atoms (C1–C6 and O2–O6) marked on the cellulose chain. Longitudes and latitudes on the damage threshold maps of Figs. 15, 16 and 17 are explained in the drawings at the bottom of Fig. 14. The markings on the maps in Figs. 15-17 show directions towards (•) and away from (×) the nearest neighbour atoms.

6.1.1 Polyethylene

Based on our DTE simulations, the average energy needed to create damage in the PE sample was 10.2±.2 eV for H recoils, and 19.9±.4 eV for C recoils. This agrees well with TEM experiments, according to which the electron energy needed to induce defects in polyethylene is about 100 keV [32], corresponding to a maximal energy transfer of 20 eV to a carbon atom. On the other hand, a 100 keV electron energy corresponds to a maximum energy transfer of 240 eV to H atoms, i.e. well above the threshold. The fact that no damage is observed in TEMs is most likely due to the fact that almost all the

damage produced by H recoils are H radicals or H_2 molecules (see also Fig. 18 on page 36) and thus not normally visible in TEMs.

Figure 15 displays the energy landscapes of the damage threshold energy for a carbon atom (a) and a hydrogen atom (b) in a polyethylene chain. Both damage threshold energy maps are based on 500 recoil events with a random initial recoil direction.

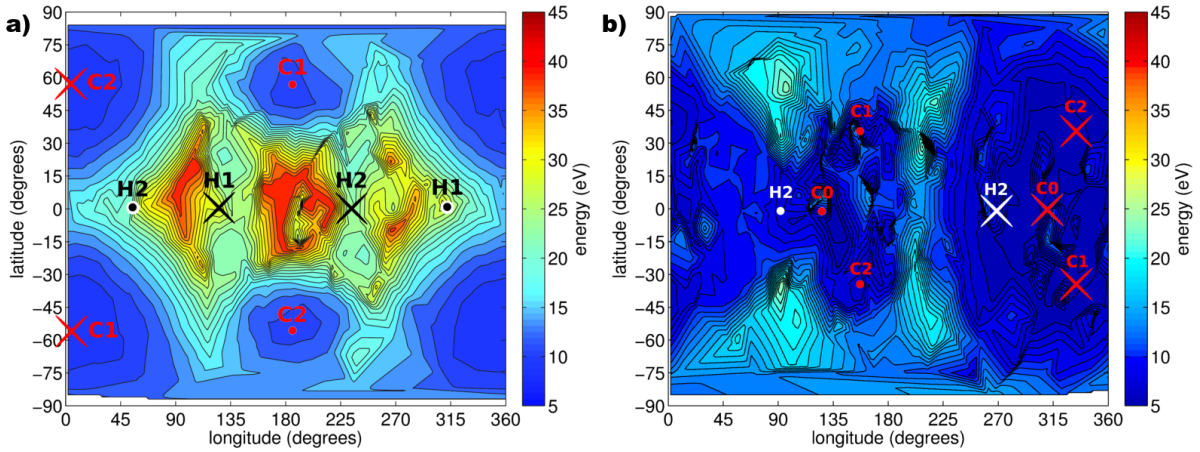

Figure 15: Damage threshold energy map for a carbon atom (a) and a hydrogen atom (b) in HDPE. The markings show directions towards (•) and away from (×) the nearest neighbour atoms.

The DTE map for a C atom in HDPE in Fig. 15a shows threshold energy values ranging from 8.8 eV to 40 eV. Creating damage requires most energy when the recoil pushes the target atom between its carbon neighbours, or perpendicular to that direction in the equatorial zone of the map. On the other hand, damage is created with the lowest recoil energies when the carbon atom is pushed along the direction of its C-C bonds. In these cases, most of the recoil energy is used for breaking a single C-C bond, instead of dividing it more evenly between two C-C bonds. Generally damage is more easily created by recoils along the chain direction (towards poles) than by recoils perpendicular to the chain direction. The C-H bonds in HDPE are rarely broken as a result of C recoils with energies less than 30 eV [73]. Thus the features of the DTE map in Fig. 15a are mostly not connected to the H1 and H2 directions.

The damage threshold map for a hydrogen atom in HDPE is shown in Fig. 15b. Since the color scale is the same as in Fig. 15a, one immediately notices that, on average, the threshold energy for creating damage by hydrogen recoils is considerably lower than the threshold energy for carbon. The lowest threshold energies for a hydrogen atom are 4.5 eV and the highest 25 eV.

Damage is created with the lowest energies when the hydrogen atom is kicked away from the nearest carbon atoms (C0, C1 and C2) or pushed towards them. When damage is

created it typically means that the recoiling hydrogen breaks its H-C bond. In about 4% of the cases the damage is caused by the neighbour hydrogen (H2 in the Fig. 14) breaking free from C1, and in about 2% of the cases the first damage to occur is the breaking of the PE chain.

6.1.2 Cellulose

Table 3 collects all the average damage threshold energy (DTE) values for each of the unique carbon (C1–C6) and oxygen (O2–O6) atoms in the cellulose monomer, and also the average DTEs for all C atoms, all O atoms, H bound to C atoms, and for H bound to O atoms.

Table 3: Average threshold energies for each unique carbon and oxygen atom in cellulose monomer, and also averages over all C, O and H atoms. The uncertainties reported in the table correspond to 1σ confidence interval.

Atom	DTE (eV)	DTE_{min} (eV)	DTE_{max} (eV)	Atom	DTE (eV)	DTE_{min} (eV)	DTE_{max} (eV)
C1	**15.4±.2**	7.1	28.5	-	-	-	-
C2	**13.6±.2**	6.7	34.5	O2	**22.7±.3**	12.3	44.6
C3	**16.8±.3**	7.8	42.5	O3	**23.8±.3**	12.3	46.4
C4	**15.3±.2**	8.8	28.9	O4	**22.2±.3**	10.6	44.3
C5	**16.5±.2**	8.8	32.7	O5	**18.9±.3**	9.2	35.9
C6	**17.7±.3**	8.5	46.0	O6	**22.9±.3**	10.9	40.1
All C	**15.9±.1**	-	-	All O	**22.1±.1**	-	-
H_C	**8.6±.1**	4.1	19.8	H_O	**9.7±.2**	3.8	21.6

From carbon atoms, C6 has the highest DTE, 17.7±.3 eV. This is expected since C6 is also the only carbon with two H bonds, thus it is able to form stronger bonds with C5 and O6. C2 has the lowest DTE, 13.6±.2 eV. On the other hand, C3 has a significantly higher DTE, 16.8±.3 eV, even though the bonding structure appears to be very similar to C2 (see Fig. 14 on page 29). The difference lies in the second neighbour atoms: because C1 has two oxygen bonds in comparison to C4's one oxygen bond, its ability to form strong bonds with C2 is decreased, and thus the C1–C2 bond is weaker than the bond C4–C3.

The average DTE for all oxygens, 22.1±.1 eV, is about 40 % higher than the average DTE for all carbons, 15.9±.1 eV. The DTE for oxygens in the OH groups (O2, O3 and O6) is somewhat higher than the DTE for O4 and O5, both of which have two O-C bonds. Maybe surprisingly, O4 has a higher DTE than O5 even though they both have a similar bonding structure. This difference appears to be due to the glucose ring often folding open after a recoil impact to O5, thus preventing the broken bond from healing, whereas

after O4 recoil, unless both O-C bonds are broken, the single dangling bond often heals itself.

Hydrogen atoms bound to O, H_O in Table 3, seem to have on average a higher DTE than hydrogen bound to C, H_C in Table 3: 9.7±.1 eV vs. 8.6±.1 eV. This agrees well with experimental bond dissociation energies: 4.7 eV for O-H and $3.5 - 4.5$ eV (affected by substituents) for C-H bonds [14]. The DTE for H_C is also slightly lower than the DTE for hydrogens in PE, 10.2±.1 eV [73].

In the damage threshold simulations the threshold energy for damage production as a function of the recoil direction was modelled for all unique carbon and oxygen atoms in a cellulose chain. The resulting DTE maps are shown in Figures 16 and 17.

Figure 16 shows DTE maps for carbon atoms C1–C6. These maps show that the damage is usually produced with the lowest energies when the recoil atom is pushed either towards its neighbour atom or directly away from it, and the map features are very similar in both of these directions. A notable exception to this is the C5–C6 bond, (in both maps at the bottom row of Fig. 16) for which the DTE is highest when C6 is kicked in the direction of C5 or when C5 is kicked away from C6, and in the respective opposite directions we see low DTE values.

DTE maps for oxygen atoms O2–O6 are shown in Fig. 17. In all maps, the threshold energy appears to be the lowest when the oxygen recoil atom is pushed away from its carbon neighbour. The DTE maps for O5 and O6 are rather symmetrical along the O-C bond directions, since a blue low threshold region is visible in both directions along the bond axis. In the DTE maps for O2–O4, the opposite trend appears, as the direction towards the neighbouring C atoms appear to be a region of high threshold energy.

6.1.3 Discussion

The average threshold energy for all C atoms in the cellulose monomer, 15.9±.1 eV, (and even the highest DTE 17.7±.3 eV for C6), is lower than the DTE for carbon atoms in HDPE 19.9±.4 eV [73]. The main reason is that the bond structure is different, as all carbon atoms in cellulose have at least one oxygen bond, although it cannot be ruled out that minor differences in the inter-atomic potentials used for polyethylene [86, 17] and cellulose [59, 44] may be in part responsible for the difference.

The minimum threshold energies reported here for C and H atoms in HDPE, and C, H and O atoms in cellulose are considerably higher than the bond dissociation energies for the corresponding bonds. E.g., for C atoms in cellulose, the DTE is 15.9±.01 eV and the bond energies for C-C and C-O bonds in cellulose are between 3 and 4 eV [44], depending on the bonding environment. A similar effect can be seen in other materials, such as Si: $E_{bond} = 2.3$ eV, $E_{thresh} = 13$ eV [52] and Fe: $E_{bond} = 1.1$ eV, $E_{thresh} = 16 - 20$ eV [53, 55].

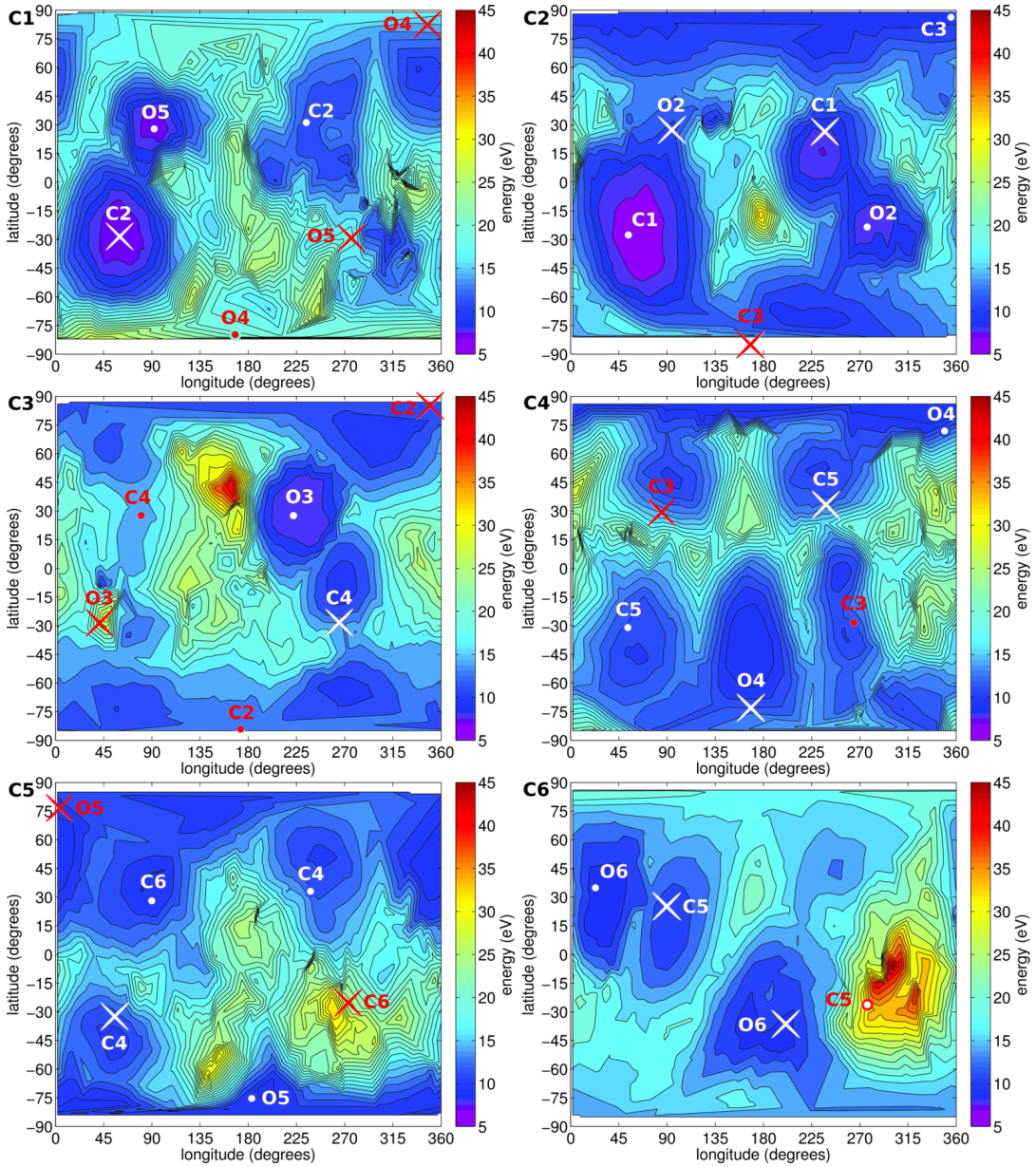

Figure 16: 2D energy landscapes showing the damage threshold energies of carbon atoms the cellulose monomer.

In graphene the bond energy is $E_{bond} \approx 5$ eV [37] and the minimum threshold energy is approximately 15.7 eV [57].

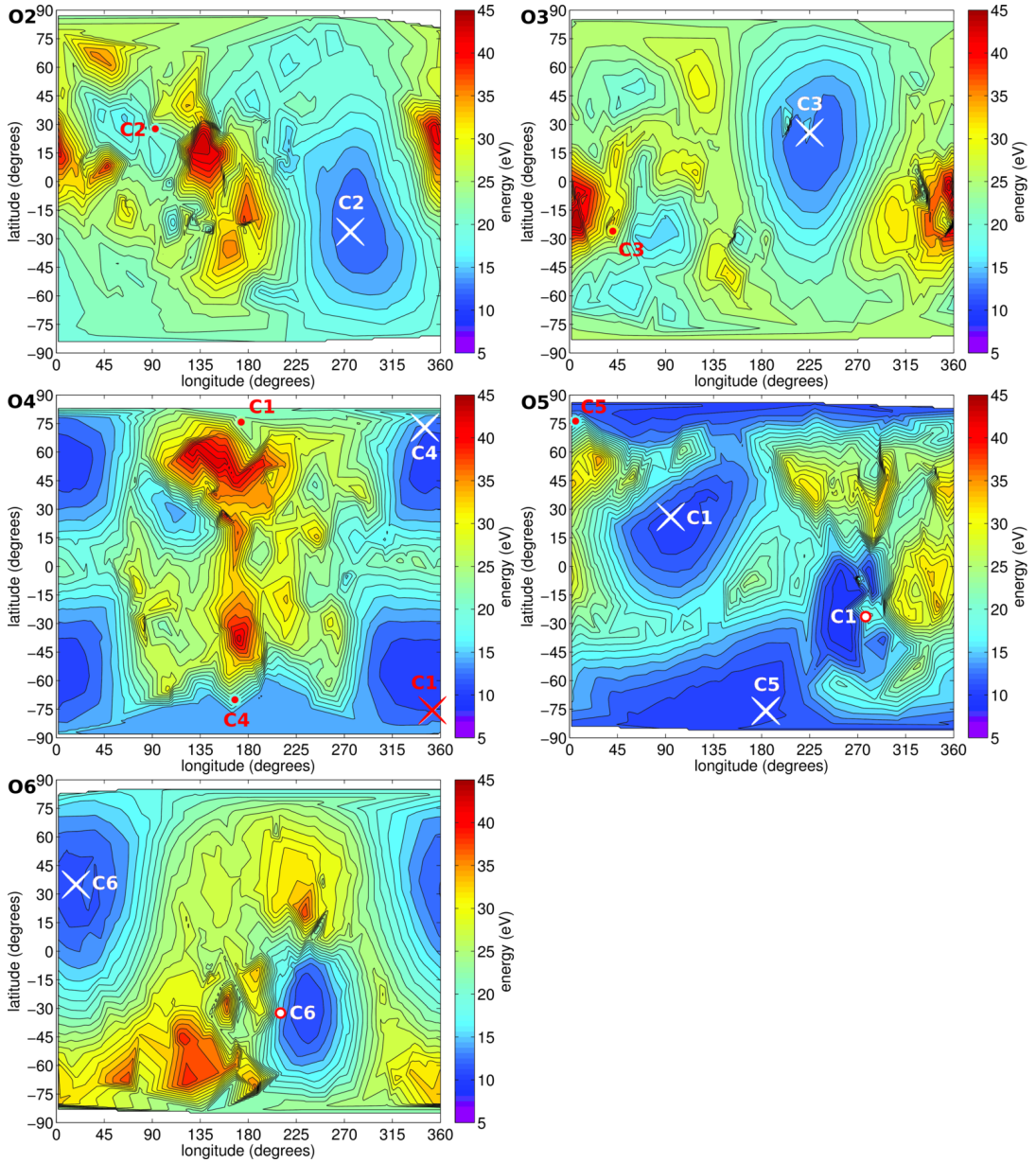

Figure 17: 2D energy landscapes showing the damage threshold energies of oxygen atoms in the cellulose monomer.

6.2 Damage production above the threshold energy

In this section the results from irradiation simulations with recoil energies above the threshold energy are reported and some comparisons between HDPE and cellulose results are made. The results in this section are mostly from publications **II** and **V**.

6.2.1 Polyethylene

Single impact simulations

Table 4 shows statistics of the different kinds of damage caused by single impact simulations at recoil energies between 5 and 100 eV. 50 hydrogen recoils and 50 carbon recoils were simulated for each energy.

Table 4: Broken chains, free molecules and cross-links formed in HDPE during single impact simulations. The uncertainties reported in the table correspond to 1σ confidence interval.

recoil energy [eV]	recoil atom	broken chains	free molecules	cross-links
5	H	0.0	0.0	0.0
	C	0.0	0.0	0.0
10	H	0.0	0.42±.09	0.0
	C	0.10±.04	0.0	0.0
20	H	0.10±.04	0.68±.12	0.0
	C	0.48±.10	0.0	0.0
30	H	0.14±.05	0.94±14	0.0
	C	0.86±.13	0.22±.07	0.0
50	H	0.24±.07	1.5±.2	0.0
	C	1.0±.1	0.58±.11	0.0
100	H	0.64±.11	2.4±.2	0.0
	C	1.5±.2	2.4±.2	0.04±.03

In single impact simulations, the damage starts to occur with 10 eV recoil energy, when approximately 10% of C recoils produce broken chains (chain scission) and more than 40% of H recoils produce free molecules. With 30 eV recoil energy all recoil events produce damage, C recoils dominantly chain scission and H recoils free radicals. Cross-linking was observed only after 100 eV C recoils. The mass of created free molecules increased linearly as a function of recoil energy (see Fig. 6 in publication **II**).

The average recoil atom path lengths[12] were from 4.6 to 14 Å for H recoils, and from 0 to 6.3 Å for C recoils, with energies of 10–100 eV. On average, the distances travelled by hydrogen recoil atoms are about twice as long as the distances travelled by carbon recoils. Even with 100 eV recoil energy, the recoiling carbon atom usually moves no farther than the nearest neighbour chain, at a 4.1 Å distance. Our MD results were

[12]The average length is calculated only from those recoil atoms that break free from the original chain.

subsequently compared with the recoil atom path lengths calculated with the binary-collision approximation code SRIM [103, 101]. SRIM calculations[13] yielded mean ranges of 14 and 47 Å for 20 and 100 eV H atoms, and 8 and 16 Å for 20 and 100 eV C atoms, respectively. Comparison with the MD results shows that the SRIM ranges are roughly a factor of 3 higher than the MD results. This indicates that the ion movement is strongly affected by the structure and chemical bonding in polyethylene, and that the binary collision approximation do not appear to be suitable for simulation of recoils in organic materials at energies $\lesssim$ 100 eV.

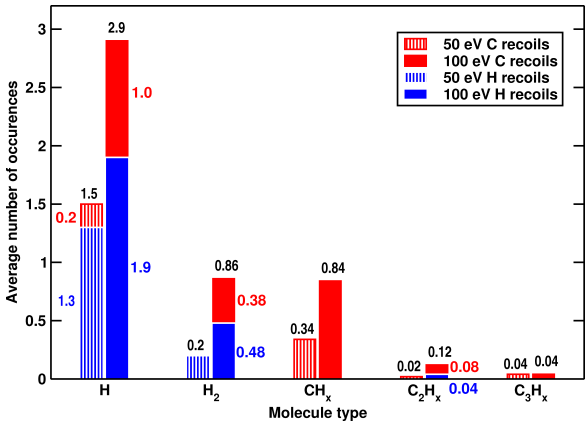

Figure 18: Distribution of free molecules from single impact simulations. Blue bars correspond to molecules created by 50 (striped) and 100 eV (full color) H recoils; red bars show the number of molecules created by C recoils.

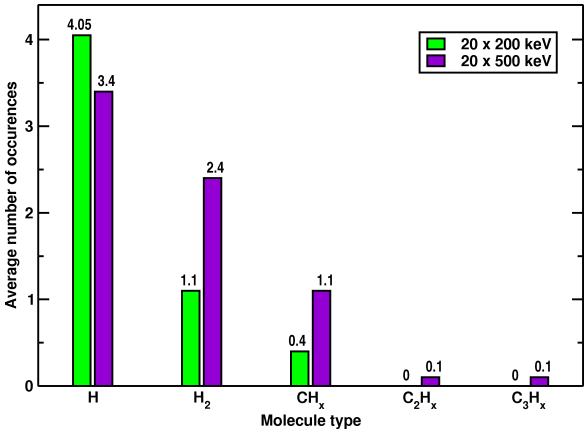

Figure 19: Average distribution of free molecules in HDPE after 20 consecutive recoils with energies corresponding to 200 (green) and 500 keV electrons (violet).

The distribution of free radicals and other molecules in 50 and 100 eV simulations is shown in Fig. 18. The most abundant radical types are H and CH_x, but some non-reactive H_2 molecules were also produced, especially by H recoils. The 100 eV recoils produced about 2.5 times more free radicals and molecules than the 50 eV recoils, namely 4.8±.3 versus 2.1±.2 radicals per recoil. The C recoils produce a wider distribution of different molecules, while H recoils create mostly H and H_2.

Cumulative bombardment

In the cumulative bombardment simulations, the effect of electron irradiation, such as TEM imaging, was modelled using electron energies of 200 and 500 keV. This means

[13]Details of parameters used can be found in publication **II**.

that the recoil atom type was chosen according to the procedure explained earlier in section 5.2, giving C or H recoils with probabilities shown in Table 5.2. The energies were given to C and H recoils according to distributions shown in Figs. 13a and 13b on page 27.

Table 5 shows broken chains, free molecules and cross-links created during the cumulative bombardment. The average recoil energy was 31.4 eV in 200 keV simulations, and 43.5 eV in 500 keV simulations. The median recoil energy values are considerably less than the averages; 17 and 18 eV for 200 and 500 keV H recoils, and 26 and 30 eV for C recoils.

Table 5: Average recoil energy and the number of broken chains, free molecules and cross-links formed in HDPE during cumulative bombardment simulations. The uncertainties reported in the table correspond to 1σ confidence interval.

electron energy [keV]	ave. recoil energy [eV]	broken chains per recoil	free molecules per recoil	cross-links per recoil
200	31.4	0.08±.02	0.28±.03	0
500	43.5	0.13±.02	0.36±.03	0

A single 200 keV electron collision during cumulative bombardment causes on average 0.08±.02 broken chains and 0.28±.03 free molecules in the target sample. For 500 keV electrons, these numbers are 0.13±.02 and 0.36±.03, respectively. Compared to the recoil events reported earlier, the damage caused by a single recoil event in the cumulative bombardment is minor. No cross-links were produced in the cumulative bombardment simulations.

The average distribution of free molecules after 20 consecutive impacts with recoil energies corresponding to 200 and 500 keV electron irradiation is shown in Fig. 19. In both cases the vast majority of free molecules are H radicals or H_2, but 500 keV electron bombardment creates a wider distribution of free molecules; H and H_2 are still most abundant but additionally there is 18% of various hydrocarbon radicals.

6.2.2 Cellulose

Single impact simulations

Table 6 shows the amount of broken chains, broken glucose rings and free molecules produced in cellulose in single impact simulations. Broken rings were found to be the most common form of damage with recoil energies 10–30 eV, and with higher recoil energies, free molecules were most abundant. Chain scission began to occur when the recoil energy was 20 eV and higher. Cross-links were formed only in one of the 100 eV simulations.

Table 6: Broken chains, broken glucose rings and free molecules formed in cellulose after single impact simulations. The uncertainties reported in the table correspond to 1σ confidence interval.

recoil energy [eV]	broken chains per recoil	broken rings per recoil	free molecules per recoil	cross-links per recoil
10	0.0	0.05±.02	0.0	0.0
20	0.07±.03	0.39±.05	0.20±.04	0.0
30	0.25±.04	0.56±.05	0.34±.05	0.0
50	0.36±.05	0.65±.05	0.85±.07	0.0
100	0.63±.05	1.1±.1	1.4±.1	0.01±.01

The distribution of free radicals and molecules produced with recoil energies of 50 and 100 eV is shown in Figure 20. With a recoil energy of 50 eV, the biggest groups of free molecules were COH_x and hydroxyl radicals (OH). With the recoil energy 100 eV, H_2 molecules form the biggest group but COH_x and hydroxyl radicals are still relatively abundant. The average amount of free molecules formed per 50 eV recoil is 0.85 and 1.4 per 100 eV recoil.

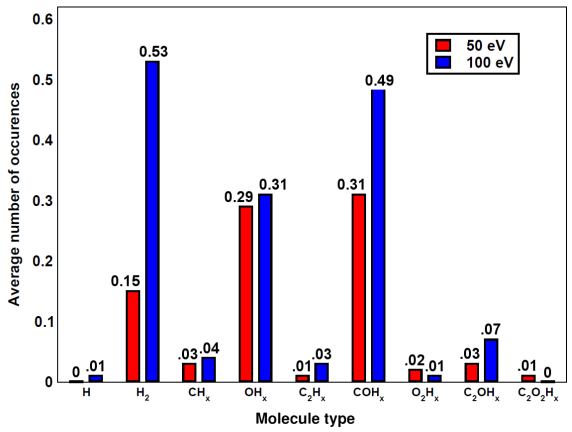

Figure 20: Distribution of free molecules from the single impact simulations of cellulose with recoil energies of 50 and 100 eV. The molecule types are ordered by increasing molecular mass.

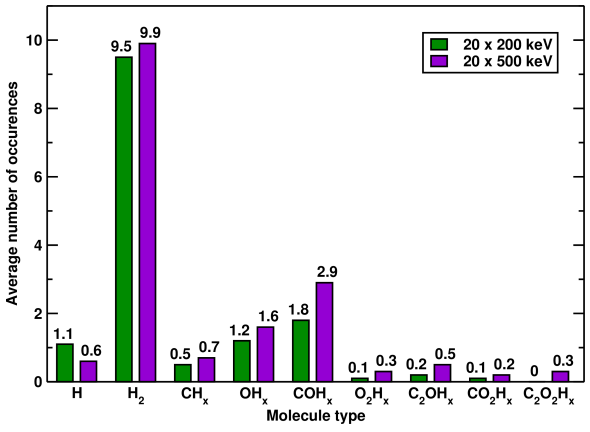

Figure 21: Average distribution of free molecules in cellulose after 20 consecutive recoils with energies corresponding to 200 keV electrons (green bars) and 500 keV electrons (violet bars).

The C and O recoils were found to have mostly similar impacts in our simulations. The biggest differences were in the amounts of radicals of form CH_x, which were all produced by C recoils, and hydroxyl radicals (OH), of which 85% were produced by O recoils.

Cumulative bombardment

In the cumulative bombardment simulations for cellulose, the effect of electron irradiation was modelled using electron energies of 200 and 500 keV, just as was done with HDPE earlier. The probabilities for H, C and O recoils are shown in Table 5.2. Figures 13c and 13d on page 27 show the threshold cross-section σ_D for hydrogen (blue), carbon (red) and oxygen (green) as a function of recoil energy. The recoil energies used in the cumulative bombardment simulations were produced with these distributions.

Table 7 shows that the average recoil atom energy in 200 keV simulations was 30.6 eV, and in 500 keV simulations 37.0 eV. Also shown are the average number of broken glucose rings, broken polymer chains, free molecules and cross-links per recoil event created during the cumulative bombardment.

Table 7: Average recoil energy and the number of broken chains, broken rings, free molecules and cross-links formed per recoil event in cellulose during cumulative bombardment simulations. The uncertainties reported in the table correspond to 1σ confidence interval.

electron energy [keV]	ave. recoil energy [eV]	broken chains per recoil	broken rings per recoil	free molecules per recoil	cross-links per recoil
200	30.6	0.005±.004	0.35±.02	0.70±.03	0.05±.01
500	37.0	0.008±.004	0.50±.03	0.80±.03	0.05±.01

The most common type of damage in the cumulative bombardment simulations is the generation of free molecules, mostly hydrogens. With 200 keV, 75% of free molecules are either H or H_2 and with 500 keV, 66%. Broken rings are formed after 35% of the 200 keV simulations and after 50% of the 500 keV simulations.

Chain scission was observed to be a rarer phenomenon with the simulated recoil energies. As we can see from Table 7, only 0.005±.004 and 0.008±.004 broken chains per recoil event were observed with 200 and 500 keV electron energies. 0.05±.01 cross-links per recoil event were produced with both electron energies.

Figure 21 shows the average distribution of free molecules after cumulative bombardment with recoil energies corresponding to 200 keV and 500 keV electron irradiation. Both simulation sets produce very similar distributions of free molecules, the main difference being that heavier fragments are more abundant after 500 keV electron bombardment.

6.2.3 Discussion

Cumulative bombardment of HDPE produced on average less damage per recoil than an event in single impact simulations with corresponding recoil energy. The reason for this

is that the recoil energy distributions used here (shown in Fig. 13) are peaked at the lowest recoil energies and thus the majority of the recoil events have such low energies that producing damage is unlikely.

In both materials, H radicals and H_2 are the most abundant free molecules formed in the cumulative bombardment simulations. This is to be expected since the recoil atoms are mostly hydrogens and from single impact results (Fig 18 in page 36) we see that H recoils produce mostly H and H_2.

Tables 5 and 7 show that, even though the electron energy increases from 200 to 500 keV (by 250%), the average recoil energy is increased much less than that, by ∼40% in HDPE and by ∼20% in cellulose. This is partly a result of the fact that with the higher electron energy, a relatively bigger fraction of recoil atoms are carbon or oxygen atoms, and the maximum energy transfer from the incoming electron to the recoil atom gets smaller as the recoil atom mass increases.

The occurrence of chain scission was found to be rare in cellulose, especially in cumulative bombardment simulations. One reason for this is that only O4 recoils are typically able to cause broken chains and only 2.1% of the recoils in the 200 keV simulations (4.2% with 500 keV) are given to this atom, and many of those do not have enough energy to produce damage. The other is that the longer simulation time (20 × from 3 to 10 ps, depending on the recoil energy) gives the broken chains formed in the earlier phases of the cumulative bombardment time to recombine or to form cross-links with neighbouring chains.

In cellulose, cross-linking was found to be more common after cumulative bombardment than after single impact simulations. A more careful analysis of the cumulative simulation systems reveals that the first three of the consecutive recoil events did not produce cross-links in any of the systems but after that they became more common. This agrees well with experiments, according to which cross-linking in the amorphous phase is more probable because of already existing disorder and irregularity among the polymer chains [83]. For instance the level of cross-linking within crystalline regions of HDPE has been reported to be about one fourth of that in amorphous regions [82].

Our cumulative bombardment results are also in qualitative agreement with Fourier transform-infrared (FT-IR) spectroscopy [38] results on irradiation of wood and cellulose which show that the material undergoes changes in the carbon bonding environment on exposure to plasmas [64, 7] and electron beams [78]. Since the type of irradiation and sample sizes are very different, a quantitative comparison with the FT-IR results is not possible.

7 CONCLUSIONS

The results presented in this thesis estimate the probability and nature of damage produced by low-energy recoils in high-density, crystalline polyethylene and in crystalline cellulose Iβ. Our results show that the threshold energy for damage production is strongly dependent on the direction of the initial recoil with respect to the covalent bonds to the neighbouring C and O atoms. The lowest threshold energy is typically observed when the recoil atom is kicked in the directly opposite direction from one of its bonded neighbouring atoms.

In HDPE, the simulated threshold energy for C atoms, 19.9±.4 eV, is in excellent agreement with TEM experiments [32]. In cellulose, the simulated threshold energies for carbon atoms were somewhat lower than in HDPE: the DTE for C atoms on the glucose ring (C1–C5) was on average 15.5 eV, and the DTE for C6, with two C-H bonds, was 17.7±.3 eV. Also, the oxygen atom on the glucose ring O5 had a lower DTE (18.9 eV) than other oxygen atoms (on average 22.9 eV).

In simulations of irradiation in HDPE with recoil energies above the threshold energy, single C recoils up to 100 eV were found to produce predominantly free H atoms and H_2 molecules, but also a significant fraction of free hydrocarbon molecules. Single H recoils produced solely hydrogen damage with recoil energies up to 50 eV, and also with 100 eV recoils the fraction of hydrocarbon radicals is only a few percent.

Two sets of cumulative bombardment simulations, with recoil energies corresponding to TEM imaging with 200 and 500 kV voltage, were carried out for HDPE and cellulose. The results showed that the most common damage types were formation of H radicals and H_2 molecules. Chain scission, cross-linking and formation of heavier radicals were observed to be less common. Consecutive recoil impacts on the same system did not produce more damage per recoil event in comparison to the single impact simulations. Although, in cellulose, the accumulated damage increased the probability for cross-linking. In HDPE, cross-linking was observed only for 100 eV C recoils, and even for these the probability was only a few percent. This agrees well with the work of Patel and Keller (1975) who concluded that in the case of crystalline HDPE, cross-linking occurs at the chain ends, not within the crystal [67].

Since it has been observed that irradiation sufficient to cause cross-linking at ambient temperature in the amorphous phase of polymeric materials (like in the case of polyethylene) produces only minor changes in the crystalline phase [1], it would be an interesting topic for future work to simulate HDPE and cellulose with amorphous regions, and study how this would affect the probabilities for chain scission and cross-linking. Another topic of interest would be to check whether density functional theory calculations would yield similar results as our threshold energy simulations.

References

[1] Adler, G. Cross-linking of polymers by radiation. *Science 141*, 3578 (1963), 321–329.

[2] Alder, B. J., and Wainwright, T. Studies in molecular dynamics. I. General method. *The Journal of Chemical Physics 31* (1959), 459.

[3] Allen, M. P., and Tildesley, D. J. *Computer Simulation of Liquids*. Oxford University Press, Oxford, England, 1989.

[4] Anand, P., Kunnumakara, A., Sundaram, C., Harikumar, K., Tharakan, S., Lai, O., Sung, B., and Aggarwal, B. Cancer is a preventable disease that requires major lifestyle changes. *Pharmaceutical Research 25*, 9 (2008), 2097–2116.

[5] Andersen, H. The depth resolution of sputter profiling. *Applied Physics 18*, 2 (1979), 131–140.

[6] Atalla, R. H., and Vanderhart, D. L. Native cellulose: a composite of two distinct crystalline forms. *Science 223*, 4633 (1984), 283–285.

[7] Avramidis, G., Hauswald, E., Lyapin, A., Militz, H., Viöl, W., and Wolkenhauer, A. Plasma treatment of wood and wood-based materials to generate hydrophilic or hydrophobic surface characteristics. *Wood Material Science and Engineering 4*, 1-2 (2009), 52–60.

[8] Avramidis, G., Klarhöfer, L., Maus-Friedrichs, W., Militz, H., and Viöl, W. Influence of air plasma treatment at atmospheric pressure on wood extractives. *Polymer Degradation and Stability 97*, 3 (2012), 469 – 471.

[9] Avramidis, G., Militz, H., Avar, I., Viöl, W., and Wolkenhauer, A. Improved absorption characteristics of thermally modified beech veneer produced by plasma treatment. *European Journal of Wood and Wood Products 70*, 5 (2012), 545–549.

[10] Baeurle, S. A., Hotta, A., and Gusev, A. A. On the glassy state of multiphase and pure polymer materials. *Polymer 47*, 17 (2006), 6243 – 6253.

[11] Beardmore, K. Ion-bombardment of polyethylene. *Nuclear Instruments and Methods in Physics Research B 102* (1995), 223–227.

[12] Bente, M., Avramidis, G., Förster, S., Rohwer, E., and Viöl, W. Wood surface modification in dielectric barrier discharges at atmospheric pressure for

creating water repellent characteristics. *Holz als Roh- und Werkstoff 62*, 3 (2004), 157–163.

[13] Berendsen, H. J. C., Postma, J. P. M., van Gunsteren, W. F., DiNola, A., and Haak, J. R. Molecular dynamics with coupling to an external bath. *Journal of Chemical Physics 81* (1984), 3684–3690.

[14] Blanksby, S. J., and Ellison, G. B. Bond dissociation energies of organic molecules. *Accounts of Chemical Research 36*, 4 (2003), 255–263.

[15] Bouchard, J., Methot, M., and Jordan, B. The effects of ionizing radiation on the cellulose of woodfree paper. *Cellulose 13*, 5 (2006), 601–610.

[16] Brenner, D. W. Empirical potential for hydrocarbons for use in simulating chemical vapor deposition of diamond films. *Physical Rewiev B 42* (1990), 9459–9471.

[17] Brenner, D. W., Shenderova, O. A., Harrison, J. A., Stuart, S. J., Ni, B., and Sinnott, S. B. A second-generation reactive empirical bond order (rebo) potential energy expression for hydrocarbons. *Journal of Physics: Condensed Matter 14*, 4 (2002), 783–802.

[18] Brown, E., Willms, R., Gray, G.T., I., Rae, P., Cady, C., Vecchio, K., Flowers, J., and Martinez, M. Influence of molecular conformation on the constitutive response of polyethylene: A comparison of hdpe, uhmwpe, and pex. *Experimental Mechanics 47*, 3 (2007), 381–393.

[19] Ceresana Research. Market study: Polyethylene – HDPE, 2012. [Online; Accessed 4 October 2013].

[20] Ceresana Research. Market study: Polyethylene – LDPE, 2012. [Online; Accessed 5 October 2013].

[21] Ceresana Research. Market study: Polyethylene – LLDPE, 2012. [Online; Accessed 5 October 2013].

[22] Chapiro, A. Radiation chemistry of polymers. *Radiation Research Supplement 4* (1964), 179–191.

[23] Charlesby, A. *Atomic radiation and polymers*. Pergamon Press Inc., 1960.

[24] Chen, Y., Zou, H., Liang, M., and Liu, P. Rheological, thermal, and morphological properties of low-density polyethylene/ultra-high-molecular-weight polyethylene and linear low-density polyethylene/ultra-high-molecular-weight polyethylene blends. *Journal of Applied Polymer Science 129*, 3 (2013), 945–953.

[25] Chmielewski, A. G., Haji-Saeid, M., and Ahmed, S. Progress in radiation processing of polymers. *Nuclear Instruments and Methods in Physics Research Section B: Beam Interactions with Materials and Atoms 236*, 1-4 (2005), 44 – 54.

[26] Cleland, M. R., Parks, L. A., and Cheng, S. Applications for radiation processing of materials. *Nuclear Instruments and Methods in Physics Research Section B: Beam Interactions with Materials and Atoms 208* (2003), 66–73.

[27] Cowie, J. M., and Cowie, J. M. *Polymers: chemistry and physics of modern materials*. CRC Press, 1991.

[28] Desmet, G., Takács, E., Wojnárovits, L., and Borsa, J. Cellulose functionalization via high-energy irradiation-initiated grafting of glycidyl methacrylate and cyclodextrin immobilization. *Radiation Physics and Chemistry 80* (2011), 1358–1362.

[29] Driscoll, M. Electron beam irradiation of cellulose. *Radiation Physics and Chemistry 78* (2009), 539–542.

[30] Duffour, E., and Malfreyt, P. MD simulations of the collision between a copper ion and a polyethylene surface: an application to the plasma–insulating material interaction. *Polymer 45*, 13 (2004), 4565 – 4575.

[31] D'Almeida, M. L. O., Barbosa, P. d. S. M., Boaratti, M. F. G., and Borrely, S. I. Radiation effects on the integrity of paper. *Radiation Physics and Chemistry 78*, 7 (2009), 489–492.

[32] Egerton, R. F., Li, P., and Malac, M. Radiation damage in the tem and sem. *Micron 35* (2004), 399–409.

[33] Ehrenstein, G. W. *Polymeric materials: structure, properties, applications*. Hanser Verlag, 2001.

[34] Gehring, J., and Zyball, A. Radiation cross linking of polymers - status, current issuers, trends and challenges. *Radiation Physics and Chemistry 46* (1995), 931–936.

[35] Ghaly, M., Nordlund, K., and Averback, R. S. Molecular dynamics investigations of surface damage produced by keV self-bombardment of solids. *Philosophical Magazine A 79*, 4 (1999), 795.

[36] Gould, R. F. *Irradiation of Polymers*. American Chemical Society, Washington, D.C., USA, 1967.

[37] Greenwood, N. N., and Earnshaw, A. *Chemistry of Elements.* Pergamon Press, Oxford, U.K., 1984.

[38] Griffiths, P., and J. A. de Hasseth, J. *Fourier Transform Infrared Spectrometry (2nd ed.).* Wiley-Blackwell, 2007.

[39] Heiner, A. P., Sugiyama, J., and Teleman, O. Crystalline cellulose Iα and Iβ studied by molecular dynamics simulations. *Carbohydrate Research 273*, 2 (1995), 207–223.

[40] Henniges, U., Okubayashi, S., Rosenau, T., and Potthast, A. Irradiation of cellulosic pulps: Understanding its impact on cellulose oxidation. *Biomacromolecules 13*, 12 (2012), 4171–4178.

[41] Ides.com. Typical properties of polyethylene (PE), 2013. [Online; Accessed 5 October 2013].

[42] Iller, E., Kukiełka, A., Stupińska, H., and Mikołajczyk, W. Electron-beam stimulation of the reactivity of cellulose pulps for production of derivatives. *Radiation Physics and Chemistry 63*, 3 (2002), 253–257.

[43] Järvi, T. T., Mayrhofer, L., Polvi, J., Nordlund, K., Pastewka, L., and Moseler, M. Adaptive molecular decomposition: Large-scale quantum chemistry for liquids. *The Journal of Chemical Physics 138* (2013), 104108.

[44] Kemper, T. W., and Sinnott, S. B. Hyperthermal atomic oxygen and argon modification of polymer surfaces investigated by molecular dynamics simulations. *Plasma Processes and Polymers 9*, 7 (2012), 690–700.

[45] Kerry Thomas, J. Fundamental aspects of the radiolysis of solid polymers, crosslinking and degradation. *Nuclear Instruments and Methods in Physics Research Section B: Beam Interactions with Materials and Atoms 265*, 1 (2007), 1–7.

[46] Khonakdar, H. A., Jafari, S. H., Rasouli, S., Morshedian, J., and Abedini, H. Investigation and modeling of temperature dependence recovery behavior of shape-memory crosslinked polyethylene. *Macromolecular Theory and Simulations 16*, 1 (2007), 43–52.

[47] Klemm, D., Heublein, B., Fink, H.-P., and Bohn, A. Cellulose: fascinating biopolymer and sustainable raw material. *Angewandte Chemie International Edition 44*, 22 (2005), 3358–3393.

[48] Klemm, D., Philipp, B., Heinze, T., Heinze, U., and Wagenknecht, W. *General Considerations on Structure and Reactivity of Cellulose: Section 2.1–2.1. 4.* Wiley Online Library, 2004.

[49] Kovalev, G. V., and Bugaenko, L. T. On the crosslinking of cellulose under exposure to radiation. *High Energy Chemistry 37*, 4 (2003), 209–215.

[50] Ku, H., Wang, H., Pattarachaiyakoop, N., and Trada, M. A review on the tensile properties of natural fiber reinforced polymer composites. *Composites Part B: Engineering 42*, 4 (2011), 856 – 873.

[51] Kurtz, S. M. *The UHMWPE handbook: ultra-high molecular weight polyethylene in total joint replacement.* Access Online via Elsevier, 2004.

[52] Loferski, J., and Rappaport, P. Radiation damage in Ge and Si detected by carrier lifetime changes: Damage thresholds. *Physical Review 111* (1958), 432.

[53] Lucasson, P. G., and Walker, R. M. Production and recovery of electron-induced radiation damage in a number of metals. *Physical Review 127*, 2 (1962), 485.

[54] Maczulak, A. E. *Renewable energy: sources and methods.* Infobase Publishing, 2010.

[55] Maury, F., Biget, M., Vajda, P., Lucasson, A., and Lucasson, P. Anisotropy of defect creation in electron-irradiated iron crystals. *Phys. Rev. B 14*, 12 (1976), 5303.

[56] McKinley Jr, W. A., and Feshbach, H. The coulomb scattering of relativistic electrons by nuclei. *Physical Review 74*, 12 (1948), 1759.

[57] Meyer, J. C., Eder, F., Kurasch, S., Skakalova, V., Kotakoski, J., Park, H. J., Roth, S., Chuvilin, A., Eyhusen, S., Benner, G., Krasheninnikov, A. V., and Kaiser, U. Accurate measurement of electron beam induced displacement cross sections for single-layer graphene. *Physical Review Letters 108* (5 2012), 196102.

[58] Nemţanu, M. R., Minea, R., and Mitru, E. Electron beam influence on microcrystalline cellulose. In *AIP Conference Proceedings* (2007), vol. 899, p. 791.

[59] Ni, B., Lee, K.-H., and Sinnott, S. B. A reactive empirical bond order (REBO) potential for hydrocarbon–oxygen interactions. *Journal of Physics: Condensed Matter 16*, 41 (2004), 7261.

[60] Nishiyama, Y., Sugiyama, J., Chanzy, H., and Langan, P. Crystal structure and hydrogen bonding system in cellulose iα from synchrotron x-ray and neutron fiber diffraction. *Journal of the American Chemical Society 125*, 47 (2003), 14300–14306. PMID: 14624578.

[61] Nordlund, K. Molecular dynamics simulation of ion ranges in the 1 – 100 keV energy range. *Comput. Mater. Sci. 3* (1995), 448.

[62] Nordlund, K., 2006. parcas computer code. The main principles of the molecular dynamics algorithms are presented in [63, 35]. The adaptive time step and electronic stopping algorithms are the same as in [61].

[63] Nordlund, K., Ghaly, M., Averback, R. S., Caturla, M., Diaz de la Rubia, T., and Tarus, J. Defect production in collision cascades in elemental semiconductors and fcc metals. *Phys. Rev. B 57*, 13 (1998), 7556–7570.

[64] Odrášková, M., Ráheľ, J., Zahoranová, A., Tiňo, R., and Černák, M. Plasma activation of wood surface by diffuse coplanar surface barrier discharge. *Plasma Chemistry and Plasma Processing 28*, 2 (2008), 203–211.

[65] O'Sullivan, A. C. Cellulose: the structure slowly unravels. *Cellulose 4*, 3 (1997), 173–207.

[66] Park, S., Baker, J. O., Himmel, M. E., Parilla, P. A., and Johnson, D. K. Research cellulose crystallinity index: measurement techniques and their impact on interpreting cellulase performance. *Biotechnol. Biofuels 3* (2010), 1–10.

[67] Patel, G. N., and Keller, A. Crystallinity and the effect of ionizing radiation in polyethylene, I. Crosslinking and the crystal core. *J Polym Sci: Polym Phys 13* (1975), 303–321.

[68] Paul, H. A comparison of recent stopping power tables for light and medium-heavy ions with experimental data, and applications to radiotherapy dosimetry. *Nuclear Instruments and Methods in Physics Research Section B: Beam Interactions with Materials and Atoms 247*, 2 (2006), 166 – 172.

[69] Perez, C. J. The effect of post-irradiation annealing on the crosslinking of high-density polyethylene induced by gamma-radiation. *Radiation Physics and Chemistry 79* (2010), 710–717.

[70] Piringer, O., and Baner, A. *Plastic Packaging: Interactions with Food and Pharmaceuticals*. Wiley, 2008.

[71] Polvi, J., Luukkonen, P., Järvi, T. T., Kemper, T. W., Sinnott, S. B., and Nordlund, K. Primary radiation defect production in polyethylene and cellulose. *J. Phys. Chem. B 116* (2012), 13932–13938.

[72] Polvi, J., and Nordlund, K. Comparison of low-energy β radiation effects in polyethylene and cellulose by molecular dynamics simulations. *NIMB Proceedings* (2013). Accepted for publication.

[73] Polvi, J., and Nordlund, K. Irradiation effects in high-density polyethylene. *Nuclear Instruments and Methods in Physics Research Section B: Beam Interactions with Materials and Atoms 312* (2013), 54 – 59.

[74] Polvi, J., and Nordlund, K. Low-energy irradiation effects in cellulose. *J. Appl. Phys.* (2013). Submitted for publication.

[75] Polvi, J., and Nordlund, K. Self-recoil irradiation effects in crystalline polyethylene. In *Proceedings of the 2013 Ion-Solid Interactions conference*, vol. 2. Moscow aviation institute publisher, Moscow, Russia, 2013, pp. 69–73.

[76] Przybytniak, G., and Nowicki, A. Evaluation of polymers designed for radiation processing. *NUKLEONIKA 53(Suppl. 2)* (2008), s67–s72.

[77] Rahman, A. Correlations in the motion of atoms in liquid argon. *Phys. Rev. 136* (10 1964), A405–A411.

[78] Said, H. M., Alla, S. G. A., and El-Naggar, A. W. M. Synthesis and characterization of novel gels based on carboxymethyl cellulose/acrylic acid prepared by electron beam irradiation. *Reactive and Functional Polymers 61*, 3 (2004), 397 – 404.

[79] Shanks, R., and Amarasinghe, G. Crystallisation of blends of lldpe with branched vldpe. *Polymer 41*, 12 (2000), 4579 – 4587.

[80] Shiraishi, N., Aoki, T., Norimoto, M., and Okumura, M. Make cellulosics thermoplastic. *Chemtech 13*, 6 (1983), 366–373.

[81] Sigmund, P. *Stopping of heavy ions: a theoretical approach.* Springer, 2004.

[82] Singh, A. Irradiation of polyethylene: Some aspects of crosslinking and oxidative degradation. *Radiation Physics and Chemistry 56*, 4 (1999), 375 – 380.

[83] Singh, A. Irradiation of polymer blends containing a polyolefin. *Radiation Physics and Chemistry 60*, 4 (2001), 453–459.

[84] Sjöström, E. *Wood chemistry: fundamentals and applications.* Academic Press, San Diego, USA, 1993.

[85] Stein, H. L. Ultrahigh molecular weight polyethylenes(uhmwpe). *ASM International, Engineering Plastics. Engineered Materials Handbook, 2* (1988), 167–171.

[86] Stuart, S. J. A reactive potential for hydrocarbons with intermolecular interactions. *Journal Of Chemical Physics 112* (2000), 6472–6486.

[87] Swope, W. C., Andersen, H. C., Berens, P. H., and Wilson, K. R. A computer simulation method for the calculation of equilibrium constants for the formation of physical clusters of molecules: Application to small water clusters. *The Journal of Chemical Physics 76* (1982), 637.

[88] Takács, E., Wojnárovits, L., Borsa, J., Fodváry, C., Hargittai, P., and Zold, O. Effect of γ-irradiation on cotton-cellulose. *Radiation Physics and Chemistry 55* (1999), 663–666.

[89] Tersoff, J. Empirical interatomic potential for carbon, with applications to amorphous carbon. *Phys. Rev. Lett. 61* (1988), 2879–2882.

[90] Van Duin, A. C., Dasgupta, S., Lorant, F., and Goddard, W. A. Reaxff: a reactive force field for hydrocarbons. *The Journal of Physical Chemistry A 105*, 41 (2001), 9396–9409.

[91] Viöl, W. Method for modifying wooden surfaces by electrical discharges at atmospheric pressure, November 2004. Patent US6818102 B1.

[92] Walton, D. J., and Lorimer, J. P. *Polymers*. Oxford University Press,, New York, USA, 2000.

[93] Wencka, M., Wichlacz, K., Kasprzyk, H., Lijewski, S., and Hoffmann, S. K. Free radicals and their electron spin relaxation in cellobiose. X-band and W-band ESR and electron spin echo studies. *Cellulose 14* (2007), 183–194.

[94] Wieland, S. Public presentation at the 18th conference on surface modification of materials by ion beams (SMMIB2013), Kusadasi, Turkey 2013.

[95] Wikipedia. Branching (polymer chemistry), 2013. [Online; Accessed 5 October 2013].

[96] Wikipedia. Vulcanization, 2013. [Online; Accessed 5 October 2013].

[97] Wolkenhauer, A., Avramidis, G., Cai, Y., Militz, H., and Viöl, W. Investigation of wood and timber surface modification by dielectric barrier discharge at atmospheric pressure. *Plasma Processes and Polymers 4*, S1 (2007), S470–S474.

[98] Yang, G., Zhang, Y., Wei, M., Shao, H., and Hu, X. Influence of γ-ray radiation on the structure and properties of paper grade bamboo pulp. *Carbohydrate Polymers 81*, 1 (2010), 114–119.

[99] Yermolenko, O., Kornich, G., and Betz, G. Molecular dynamics simulation of sputtering of metal clusters on polyethylene surface. *Bulletin of the Russian Academy of Sciences: Physics 74*, 2 (2010), 114–117.

[100] Yoshiharu, N. Crystal structure and hydrogen-bonding system in cellulose Iβ from synchroton x-ray and neutron fiber diffraction. *Journal of the American Chemical Society 124*, 31 (2002), 9074–9082.

[101] Ziegler, J. F. SRIM-2008.04 software package, available online at *http://www.srim.org*.

[102] Ziegler, J. F., Biersack, J. P., and Littmark, U. *The Stopping and Range of Ions in Matter*. Pergamon, New York, 1985.

[103] Ziegler, J. F., Biersack, J. P., and Ziegler, M. D. *SRIM - The Stopping and Range of Ions in Matter*. SRIM Co., Chester, Maryland, USA, 2008.